An interface of genetically engineered human forebrain assembloids and polymeric nanofiber scaffolds for multiscale profiling of interneuron migration disorders

Riya Rauthan (rauthan.riya@gmail.com)
CSIR IGIB
Vishal Bharti
CSIR IGIB
Atharva Agashe
Virginia Tech
Praveen Singh
CSIR IGIB
Harrison M York
Monash Biomedicine Discovery Institute
Amrinder S. Nain
Virginia Tech.
Senthil Arumugam
Monash Biomedicine Discovery Institute
Debojyoti Chakraborty
CSIR IGIB

Research Article

Keywords:

Posted Date: January 5th, 2024

DOI: https://doi.org/10.21203/rs.3.rs-3831019/v1

Additional Declarations: The authors declare no competing interests.

Abstract

Neuronal migration is a fundamental process during brain development in which different types of neurons migrate from their place of origin to the site where they reside and make networks crucial for the formation of proper brain architecture and its overall function. Interneuron migration anomalies due to genetic or environmental perturbations can lead to malfunctions in the neural circuitry and are observed in the case of multiple neuropsychiatric conditions. Variants in Erb-B2 Receptor Tyrosine Kinase 4 (ERBB4), a member of Tyr *protein* kinase family and the epidermal growth factor receptor subfamily that functions as a surface receptor in interneurons, have been associated with human neurodevelopment disorders such as schizophrenia, epilepsy, and intellectual disability. Animal studies elucidate the function of *ERBB4* in neuronal migration, synaptogenesis, synaptic transmission, and plasticity. However, the exact mechanistic role of *ERBB4* in the migration of GABAergic cortical interneurons in humans is unidentified. In this study, we employ CRISPR/Cas9 to knockout *ERBB4* in human induced pluripotent stem cells and report its effect on the phenotype and global gene expression upon deriving dorsal and ventral human forebrain identity organoids. Additionally, fluorescent reporter knock-in using CRISPR/Cas9 at an interneuron-specific marker in the same hiPS cell line allowed distinct temporal fluorescence expression in the derived ventral forebrain organoids allowing the capture of tangential migration of labeled cortical interneurons in intact fused 3D assembloids, to pinpoint the role of *ERBB4* in migration and function of these neurons. To capture the changes in migration dynamics of individual *ERBB4*$^{-/-}$ interneurons in high resolution, we recapitulated the migration behaviour. on nanofiber scaffolds that mimic the *in vivo* fibrous extracellular microenvironment. Our findings uncover the function of *ERBB4* in the context of human interneuron migration.

Introduction

The formation of cortical neural circuits in the human brain involves successful synaptic integration of γ-aminobutyric acidergic (GABAergic) inhibitory interneurons with glutamatergic excitatory neurons (Bartolini et al., 2013; Tatti et al., 2017). The antagonistic role of these two types of neurons is important for the functioning of their circuits. Cortical interneurons (CINs) are born from progenitors in the medial, lateral and caudal ganglionic eminence (MGE, LGE, and CGE respectively) of the ventral forebrain (telencephalon) or sub-pallium and cohorts of immature CINs in the GE region actively migrate long distances from their place of generation to reach their respective dorsal cortical layers for settlement leading to finer cortical patterning, correct lamination, and arealization of the neocortex. CINs migrate tangentially for months, starting from human embryonic gestational week 7 (Ma et al., 2013; Peyre et al., 2015; Silbereis et al., 2016). CIN tangential migration anomalies can lead to an imbalance in the excitatory and inhibitory neuronal population and malformation of neuronal circuits which contributes to the pathophysiology of neuropsychiatric disorders including schizophrenia, autism, and epilepsy (Marin, 2012). Genetic linkage and association studies have identified several genes involved in neuronal migration as candidate susceptibility genes for neurodevelopmental disorders but their underlying cellular and molecular mechanisms are still poorly understood.

ERBB4 (Erb-B2 Receptor Tyrosine Kinase 4) receptor, a member of the Tyrosine protein kinase (RTK) family and the EGFR subfamily, selectively localizes to the membrane of CINs in the developing and mature cortex and the hippocampus (Del Pino et al., 2013; Fazzari et al., 2010; Neddens & Buonanno, 2010; Vullhorst et al., 2009). Patients with *ERBB4* de novo and inherited intragenic deletion variants exhibit syndromic or non-syndromic intellectual disability, speech delay, repetitive behavior, and seizures, linking its role in cortical development (Hyder et al., 2021; Kasnauskiene et al., 2013). Previous studies have explored the role of ERBB4 in neurodevelopment by pharmacological inactivation or genetic ablation in rodent models to show the progression of schizophrenia (Chen et al., 2010; Wen et al., 2010). The chemokine ligand Neuregulin1 (NRG1) mediated ERBB4 activation is necessary for axon guidance, interneuron migration, synapse formation and network connectivity during development(Fazzari et al., 2010; Flames et al., 2004; Mei & Xiong, 2008; Shamir et al., 2012) and recently the role of ERBB4 in local translation at cell type specific synaptic connections has been established(Bernard et al., 2022). $Erbb4^{+/-}$ mice and conditional mutants have behavioral abnormalities, cognitive impairment and delayed motor development while $Erbb4^{-/-}$ is embryonically lethal (Gassmann et al., 1995). Recent findings in mice prove that early deletion of ErbB4 significantly reduces the amount of Parvalbumin positive interneurons in the postnatal cortex. Contrarily, late deletion of this gene avoids migratory problems and results in a cortex with the usual number of interneurons but aberrant brain wiring(Batista-Brito et al., 2023). Inactivation of the kinase activity of ERBB4 or its genetic ablation in postmitotic interneurons does not impair their migration into the cortex (Fazzari et al., 2010; Luo et al., 2021). Therefore, the onset of genetic dysregulation may have a significant impact on how neurodevelopmental diseases manifest clinically. Defects in interneuron migration upon ERBB4 disruption have been inferred indirectly from reduced or anomalous endpoint layer allocation of these neurons in mouse cortex (Batista-Brito et al., 2023; Hodge et al., 2019; Mayer et al., 2018) and the precise mechanistic function of *ERBB4* in tangential migration of cortical GABAergic interneurons in human brain is still unidentified.

To address this question in our study, 3D self-organizing forebrain regionalized organoids derived from human induced pluripotent stem cells (hiPSCs) have been utilized, that resemble domains of the developing cortex (Lancaster et al., 2013; Pasca et al., 2015; Quadrato et al., 2017; Yoon et al., 2019). Dorsal-ventral forebrain organoid fusion into a single assembly have contributed to the studies of functional interaction between these two subdomains of the forebrain and previously helped in dissecting the migratory behavior of human GABAergic interneurons (Bagley et al., 2017; Birey et al., 2017; Birey et al., 2022).

Here, we performed the knock-in of doxycycline-inducible Cas9 into the genomic “safe harbor” *AAVS1* for efficient genetic perturbations in human iPS cells. In this genetic background, we integrated a cell type-specific reporter to trace CINs within the forebrain assembloids to gain insights regarding the critical migration process that contributes to the excitation-to-inhibition balance in the cortex. While maintaining a physiologically relevant extracellular matrix substrate for migration (Jana et al., 2019; Jana et al., 2023; Mukherjee et al., 2023), we optimized a platform of organoids on suspended networks of uniformly

fabricated fibers, to visualize how the loss of function of *ERBB4* affects motility of migrating interneurons.

Results

CIN specific reporter tagging in hiPSCs amenable for genetic perturbations

To facilitate multiple rapid and efficient genome engineering in human iPS cells, we opted for a strategy to integrate doxycycline-inducible SpCas9 at the “safe harbor” AAVS1 locus in human IMR90 iPS cells by Homology Directed Repair (HDR) (Castano et al., 2017). To this end, we used the type II-B CRISPR–Cas9 system from *Francisella novicida* (FnCas9) which in our previous studies, showed a combination of high intrinsic target specificity and higher homology directed repair outcomes when compared with SpCas9 (Acharya et al., 2019). The donor cassette for Homology Directed Repair (HDR) contained components of TET-ON gene expression system for Cas9 with the rTetR (“reverse” Tetracycline repressor) activator driven by CAG promoter and the Tetracycline Response Element (TRE) promoter for SpCas9 (Supplementary Fig. 1a). A single guide RNA (sgRNA) was used to target FnCas9 to the intron 1 of *PPP1R12C* gene (AAVS1 site, (Mali et al., 2013)) (Fig. 1a, Methods). Puromycin antibiotic from the donor cassette allowed for the selection of iPSC clones with successful knock-in. Confirmation of genomic integration of SpCas9 in selected and propagated IMR90 hiPS cell clones was done by PCR using primers flanking the donor cassette and genome and a specific amplicon of desired size was observed in the case of knock-in clones only (Supplementary Fig. 1b-c). Finally, we confirmed the robust and tunable expression of SpCas9 upon doxycycline treatment after 48 hrs (Fig. 1b, methods) and the selected hiPSC clones also showed proper expression of pluripotency markers, OCT4 and SOX2 confirming successful generation of the iCas9 knock-in iPSC line (Supplementary Fig. 1d).

Next, we proceeded towards developing a cellular model for facilitating the identification, tracking and isolation of viable GABAergic neurons from the in vitro differentiated iPSC lines. Towards this, we attempted to integrate a fluorescent reporter that could specifically label GABAergic neurons in the iCas9 knock-in iPSCs. The enzyme glutamate decarboxylase 67 (GAD67) encoded by the GAD1 gene is responsible for synthesis of GABA inhibitory neurotransmitter as it catalyzes the production of gamma-aminobutyric acid from L-glutamic acid (Pinal & Tobin, 1998). We reasoned that tagging of GAD67, being a very early marker of the GABAergic fate with extensive expression in the soma, would enable inclusion of all diverse GABAergic interneuron subtypes encompassing those with unique developmental origins from different regions of the sub-pallium (Esumi et al., 2021). This is in contrast to previous studies where transcription factor NKX2.1 has been tagged for CIN migration assays defining only the medial ganglionic eminence (MGE) progenitors and derived GABAergic interneurons (Tamamaki et al., 2003; Yun et al., 2002). We constructed a donor DNA cassette with a P2A-mClover3 reporter and hygromycin antibiotic cassette under PGK promoter for gene targeting by doxycycline induction of SpCas9 in IMR90-iCas9 hiPS cells (Fig. 1a). The cassette was flanked by 800 bp homology arms against C-terminal of

GAD1 gene for integration before the STOP codon. We confirmed the genomic knock-in after hygromycin treatment and selection of iPSC clones, by PCR genotyping (Supplementary Fig. 1e). To characterize the expression of transgenic mClover signal in human GABAergic cortical neurons, hiPSCs were differentiated to drive the development of CINs (Fig. 1c). Upon dual SMAD inhibition for neural induction, Purmorphamine, an agonist of Smoothened receptor of the SHH pathway was added for ventral patterning (Fig. 1c). By 3 weeks of differentiation, hiPSC-derived cells expressed Nestin, a neural stem cell marker and by 30 days, NKX2.1, indicating the cell identity of MGE progenitors (Supplementary Fig. 1f-g). Importantly, CINs were differentiated in culture and by day 35 began to show faithful mClover signal suggesting proper, development-specific expression of the reporter gene (Fig. 1d). We further established the specificity of the endogenous construct expression through co-immunostaining with GAD67 and NKX2.1 followed by quantitative image analysis (Fig. 1e). Strikingly, by day 50, 90% of GAD67 + cells were also positive for mClover in the tagged group (Fig. 1f) and a sustained expression of mClover was observed in the cultured CINs. Taken together, our iPSC derived reporter cell line captures all IN subsets and can be used for imaging-based studies.

ERBB4 $^{-/-}$ forebrain organoids display reduced neuronal projections

We wanted to study the role of *ERBB4* in modulating the migration of human CINs. Hyder et al, report cases of individuals with chromosome 2q34 deletions affecting *ERBB4*, exhibiting intellectual disability in three families having genetic deletion of exon 2 (Hyder et al., 2021). In silico analysis of the outcome of exon 2 deletion shows the incorporation of a STOP codon in frame and results in a truncated protein of 40 amino acids. Such deletion might also prevent translation of the protein isoforms (Fig. 2a). Therefore, we constructed *ERBB4*$^{-/-}$ hiPSC line in the background of iCas9 GAD1-mClover by deletion of exon 2 (Wang et al 2015) (Supplementary Fig. 2a, methods). *ERBB4*$^{-/-}$ hiPS cell colonies were expanded and screened by PCR to identify pure knockout clones with genomic deletion of 436 bp confirmed by DNA sequencing (Fig. 2b, methods). The selected *ERBB4*$^{-/-}$ hiPSC clone was also characterized for pluripotency marker validation (Supplementary Fig. 2b-c). Finally, we differentiated the ECG-iPSCs into CINs and as previously observed for WT cells, these iPSCs expressed mClover by day 35 suggesting the knockout of *ERBB4* did not affect IN formation (Supplementary Fig. 2d). Importantly, western blot from cell lysate upon differentiation of *ERBB4*$^{-/-}$ iCas9_GAD1-mClover iPSC (hereafter called ECG-iPSCs) into CINs (day 35) confirmed the knockout of ERBB4 protein (Fig. 2c). Importantly the GAD67 positive cells co-stained with ERBB4 only in WT with no ERBB4 expression in *ERBB4*$^{-/-}$, confirming the specific knockout in GABAergic interneurons (Fig. 2d). Through these results, we show that human *ERBB4* is not essential for GABAergic interneuron formation under *in vitro* conditions.

Upon successful knockout of *ERBB4* in human CINs, we hypothesized that it might have a role in the migration of CINs, as speculated from mouse studies. Unlike mice, where stage specific IN migration can be examined using stained brain tissues, observing dynamic IN migration events in human brain sections is currently not feasible. To circumvent these limitations, we took help of a forebrain assembloid system by fusing two separately grown ventral and dorsal spheroids. It was expected that such a setup would

facilitate the cortical interneuron migration from ventral to the dorsal forebrain and allow us to carefully dissect modulators of CIN migration (Bagley et al., 2017; Birey et al., 2022) (Fig. 2e).

To establish a system where migratory dynamics of CINs can be accurately quantified, we introduced variations in the assembloid culture system taking inspiration from other reported methods. To enhance the onset of neuroectodermal differentiation, we used an optimized guided approach of region-specific forebrain organoid formation that involved neuroectodermal Embryoid Bodies (EBs) induced by dual-SMAD inhibition along with Wnt activation for dorsalization (Chambers et al., 2009; Sloan et al., 2018). We followed a similar approach for ventral forebrain organoid induction where dual SMAD and Wnt signaling inhibition was coupled with SHH pathway activation. For dorsal identity, SHH antagonist, CyclopamineA was added to neural induction media, and ventral/striatal identity was performed as per previously established protocol using SHH agonist and WNT antagonists during neural induction (Bagley et al., 2017) (Fig. 2e; Supplementary Fig. 2e). Upon patterning and induction of the neuroectoderm, we observed subsequent formation of the neuroepithelium in stereotypical rosette-like structures (Lancaster & Knoblich, 2014) (Supplementary Fig. 2f).

We opted for the fusion of separately patterned organoids derived from hiPSCs on day 12 in culture by seeding them in 1.5ml MCT or U-bottom plates (Sloan et al., 2018) (Supplementary Fig. 2g). This modification from previous reports (Bagley et al., 2017) resulted in a robust number of successful fusions and also allowed for easy embedding in Matrigel after 2 days to promote growth and structural organization. Dorsal forebrain organoids (DFOs) and ventral forebrain organoids (VFOs) were also cultured separately towards differentiation. A specific mClover signal was observed only from the VFOs from day 30 onwards (Supplementary Fig. 2h). To confirm the successful derivation of the forebrain identity organoids, the expression of specific markers of the ventral forebrain GE subregions was validated. FOXG1, human forebrain marker was expressed in both dorsal and ventral forebrain while GSX2 (LGE and CGE marker) level increased in the VFOs, along with NKX2.1 and LHX6 (MGE markers). In contrast, PAX6 and TBR1 expressed only in the DFOs (Supplementary Fig. 2i).

Upon starting the 3D differentiation of *ERBB4*$^{-/-}$ hiPSC line, EBs were successfully formed by aggregation of hiPSCs and were patterned to the dorsal and ventral identity (Supplementary Fig. 2j). Separately generated VFOs at week 2 were integrated with DFOs in case of both WT iPSCs and ECG-iPSCs and after 30 days of differentiation, expression of mClover was observed only in the ventral identity regions in both WT and *ERBB4*$^{-/-}$ conditions (Fig. 2f). After 50 days in culture, mClover + GABAergic cells were also observed in unlabeled (dorsal) regions of the assembloids (Fig. 2g), confirming that these cells had migrated into the dorsal cortical regions, similar to the migrating CINs during human brain development (Bagley et al., 2017; Bajaj et al., 2021). Both control and *ERBB4*$^{-/-}$ assembloids exhibited expression of dorsal radial glia progenitors, PAX6 and postmitotic neuron marker, TBR1. By week 7, both assembloids (WT and KO) expressed markers of the GE progenitors, NKX2.1; interneuron marker, GAD67 and an interneuron subtype marker, Parvalbumin (PVALB). There was insignificant change in the expression of forebrain lineage markers in *ERBB4*$^{-/-}$ hiPSC-derived assembloids over control

(Fig. 2h). In summary, the ECG-iPSCs derived assembloids exhibited the necessary hallmarks of human forebrain identity.

We observed that WT VFOs cultured in matrigel without their dorsal counterpart showed extensive neuronal projections upon neural differentiation from day 35 onwards. Strikingly, *ERBB4*$^{-/-}$ VFOs showed visibly reduced projections (Fig. 2i). Quantification of the surface area of the WT and KO organoids within the outer boundary at day 40 and day 60 revealed no difference in organoid size between the two although both organoids showed a substantial increase in the surface area from day 40 to day 60 as expected (Fig. 2j). Upon quantification of radial distance from the organoid rim, a significant decrease in the migration distance from the organoid periphery was observed in *ERBB4* KO VFOs compared with the WT VFO group (Fig. 2k-l). The identity of the projections at the organoid periphery and presence of differentiated GABAergic neurons in *ERBB4* KO, was checked by immunohistochemical staining of organoid sections which confirmed that the cells expressed GABAergic interneuron marker, GAD67 (Supplementary Fig. 2k). Thus, 3D organoid modeling displayed a lack of neuronal projections in human *ERBB4*$^{-/-}$ cortical interneurons.

Loss of ERBB4 impairs migratory properties of cortical interneurons

Next, we proceeded towards the dynamic live cell imaging of CINs in the fused assembloids. Traditionally, studies of GABAergic interneuron migration derived from 3D cultures rely on whole mount imaging or organotypic slice preparations of assembloids (Supplementary Fig. 3a, (Bajaj et al., 2021)). However, live intact assembloid imaging suffers from lower resolution due to lack of light penetration and an imaging depth of around 50–150 um only (Andersen et al., 2020; Meng et al., 2023). To determine whether our ECG-iPSC derived assembloids were amenable to live imaging, we evaluated two different methodologies. Firstly, we performed culture of organotypic slices of assembloids for time lapse imaging of migrating CINs (Supplementary Fig. 3b; Supplementary Movie 1). However, due to the fragile nature of vibratome processed cortical slice preparations from forebrain assembloids, detailed analysis of movements of cells within the slice could not be recapitulated. In addition, we faced technical difficulties associated with reproducible mechanical sectioning of soft samples like organoids and in discerning the proper orientation of fused forebrain regions. For our study, the latter was particularly critical since we specifically investigated CINS migrating towards the dorsal surface.

We then imaged the ECG-iPSCs derived assembloids using Light Sheet Microscopy (LSM), which has also been utilized to image 3D organoids but it is feasible for only small or clarified spheroid/organoid samples (Boutin et al., 2018; He et al., 2022). A persistent challenge in imaging inside live tissues is the reduced optical penetrance and low signal resolution. To this end, we experimented with optimizing signal:noise ratios through the supplementation of non-toxic Opti-prep or Iodixanol for refractive index tuning of surrounding culture media (Boothe et al., 2017). The advantage was majorly limited to relatively small-sized spheroid samples and failed with large and complicated organoids (Supplementary Fig. 3c; Supplementary Movie 2; Supplementary Table 1).

Since whole assembloid imaging wasn't able to capture CIN migration effectively, we next proceeded to dissect these parameters with greater granularity at the level of individual VFOs. Upon observation of reduced neuronal projections around the periphery of *ERBB4*$^{-/-}$ VFOs, we addressed the question of whether these interneurons show reduced motility in *in vitro* migration assays. To ascertain if ERBB4 regulates migration of human CINs, a simplified two-dimensional neurosphere outgrowth migration assay was performed. More than one millimeter sized 42-days old WT and *ERBB4*$^{-/-}$ VFOs were physically dissociated into visibly smaller aggregates and plated on PLO-Laminin coated dishes/coverslips (Supplementary Fig. 3d-e). 3 days post-attachment extensive projections of mClover + interneurons were observed moving away from the periphery of the dense WT VFO aggregate (Fig. 3a). Interneurons exhibited reduced neuronal projections around the periphery of *ERBB4*$^{-/-}$ VFO (Supplementary Fig. 3f) similar to the previous observations in matrigel. Five days post-plating migrated cells from the organoids were divided into two groups defined by the distance of migration (Fig. 3b). For comparison across different aggregates, the radial distance from the perimeter of the organoid to the outer circumference of migrated cells was calculated, and the number of interneurons that migrated from the periphery to 100 µm distance as well as beyond 100 µm distance were quantified. The motility observed showed visible differences as in the case of the *ERBB4*$^{-/-}$ interneurons. Notably, individual long projections and branching were absent and cells displayed collective cell migration outside VFO periphery (Fig. 3c). Taken together, significantly fewer *ERBB4*$^{-/-}$ interneurons could migrate to 100 µm and beyond, indicating a deficit in migration.

Next using time lapse imaging, we determined the migratory dynamics of cortical interneuron migration in high resolution, we imaged migratory dynamics of cortical interneurons and their saltation parameters on coated coverslips. Post 26 hours, we observed an increase in the population of cells close to the VFO periphery in the same field due to the proliferation of cells from VFO (Supplementary Fig. 3g). However, the overall distance migrated individually by WT interneurons was found to be lower than that observed in shorter timescales during slice culture assays (Supplementary Movie 3). Therefore, migration from solitary VFOs on coverslips even for WT CINs was inefficient. This is in close agreement with a previous report where saltatory migration of human interneurons from solitary VFOs plated on coverslips was quantified to be inefficient or absent (Birey et al., 2017).From the observations of 2D CIN migration assays, it was evident that a combination of physical substrate-driven mechano-sensation along-with intra-cellular signaling and inter-cellular interactions are crucial for the tangential migration of GABAergic CINs. Additionally, assembloid sample preparations with physical sectioning result in tissue damage and artefacts. Approaches involving slice culture in combination with optical sectioning via Single Plane Illumination Imaging (SPIM) face imaging bottlenecks owing to the thick nature of the tissue, resulting in poor resolution and contrast. To overcome these limitations, we utilized suspended fiber nano-nets, that allow 3D organoids to directly interact with polystyrene fibers (Jana et al., 2019). One of the key motivations for studying interneuron migration on these nano-nets was to interrogate single cell migratory behavior and identify subtle changes in the dynamics of *ERBB4*$^{-/-}$ migrating cells. The diameter of the suspended fibers was kept at 500 nm which is closer to the physiological ECM fiber bundles (Revell et al., 2021; Siadat et al., 2021) (Supplementary Fig. 3h). Importantly, migrating neurons

utilized the nanofibers as tracks, allowing them to migrate and separate out from the organoids. This enables characterizing migration dynamics in *ERBB4*$^{-/-}$ CIN at high resolution.

Different arrays of aligned nanonets were used to mimic the brain micro-fibrillary environment and investigate the migration of CINs from VFOs over 20 hrs (Supplementary Fig. 3i). Ventral forebrain organoids were dissociated and seeded on aligned fibers and phase contrast images were acquired every 10 min for 24 hours' time period (Supplementary Movie 4). Extensive long neurite projections and exploration of the surrounding environment on was observed in WT interneurons Our findings match the previous reports of neurite extensions on aligned fiber networks (Bakhru et al., 2011). To validate the identities of these neurons emanating from the WT VFO across various scaffolds, samples were fixed post-imaging and immunostained for GAD67 marker. Migrating cells on the fibers expressed this interneuron-specific marker (Supplementary Fig. 3j). Interestingly, long-distance migration (beyond 500 µm) of interneurons was observed on aligned fibers from the WT VFO perimeter (Fig. 3e) within 3 days of plating. In contrast, the extent of migration was absent when experiments were previously done on flat coverslip substrates. For *ERBB4*$^{-/-}$ CINs, collective persistent migration with reduced individual projections was observed (Fig. 3d; Supplementary Movie 5).

To further explore the role of underlying fiber geometry, disassociated WT VFOs were seeded on crosshatch nanonets and extensive migration was observed. Interestingly, long-distance migration of interneurons was observed on fibers of the migration scaffolds, beyond 500 µm from the WT VFO perimeter (Fig. 3e) within 3 days of plating. Such an extent of migration was absent when experiments were previously done on flat coverslip substrates. Upon using parallel orientation nano-fibers, unidirectional helical locomotion of interneurons was observed in both WT and KO interneurons with cells attaining bipolar morphology (Supplementary Movie 6; Supplementary Fig. 3n-o). To characterize the whole range of migratory behaviors, phase images of WT VFO samples were acquired every 3–5 min interval and position of interneurons tracked (Fig. 3f). Interestingly, we observed the interneurons to attain multipolar morphology and show branching of the leading process, possibly for the exploration of the extracellular fibrous environment (Fig. 3g). Migration trajectories of individual interneurons was traced and analyzed for their characteristic saltation movement. A swelling ahead of the trailing part with the nucleus behind it was observed and within three hours of swelling formation, the nucleus made a forward translocation (Fig. 3g; Supplementary Movie 7). These discontinuous saltatory movements confirmed that the behavior of these migrating cells resembled the unique GABAergic interneuron migration dynamics (Bellion et al., 2005).

After 24 hrs. of imaging, it was observed that *ERBB4*$^{-/-}$ interneurons showed decreased migration ability outside the VFO (Supplementary Movie 8) and very few interneurons could escape out of the VFO along the fiber with saltatory motion (Supplementary Fig. 3l). Interestingly, few cells showed leading projections extending onto the fibers and a trailing nucleus but were unable to perform a single nuclear translocation event (Fig. 3h). *ERBB4*$^{-/-}$ VFOs fixed on scaffolds and immunostained for interneuron marker, GAD67, showed expression in neuron projections confined within the outer rim of the organoid (Supplementary Fig. 3k). Upon quantification of saltation parameters, it was found that the length of saltation was

significantly increased for *ERBB4*$^{-/-}$ interneurons compared to the WT VFO (Fig. 3i). However, no significant difference was observed in the average migration rate of KO interneurons (Fig. 3j; 42.9 ± 4.8 μm/hr for WT; and 46.86 ± 6.5 μm/hr for KO; n = 16 cells). It has also previously been suggested that nucleokinetic speed is not a major determinant of interneuron migration due to the arrhythmic nature of motion (Nichols et al., 2008). We therefore counted the saltatory events during a defined period for both WT and *ERBB4*$^{-/-}$ CINs and found that the frequency of these nuclear translocations was reduced in the KO (Fig. 3k). Thus, the difference in mean saltation length between WT and *ERBB4*$^{-/-}$ interneurons was produced largely by increased duration of single step. Extension and retraction of branches and leading process oriented in all directions from the interneurons were observed while cells also exhibited switching from one fiber to another and changes in their direction of motion on fiber networks (Supplementary Fig. 3m, Supplementary Movie 9).

The reduced migration on fibers for *ERBB4*$^{-/-}$ CINs was striking, suggesting that ERBB4 is critical for migration of interneurons. The observed alteration of saltatory event duration resulting in nucleokinetic abnormalities could be a possible contributor to the pathological condition. Overall, our findings suggest that nanofibers are a suitable artificial ECM that can be a better mimic of physiological matrix to potentially improve screening of cell migration parameters.

ERBB4 regulates human CIN migration via RHOA/RAC1 signaling

To further address the exact role of ERBB4 and associated signaling pathways in human CIN migration, bulk transcriptomics of ventral:dorsal organoid fusions at day 60 time point was performed. This time point for study was chosen since mClover expressing cells were observed by day 35 in the assembloids in culture and also increased migration was observed from day 40–60 in control assembloids similar to previous reports (Bagley et al., 2017). Principal component analysis (PCA) performed on the whole transcriptome of assembloids at day 60 showed distinct separation of control versus knockout samples from different assembloid batches (Supplementary Fig. 4a) Out of the total differentially expressed genes, 3,868 genes were downregulated and 3,277 genes were upregulated in *ERBB4*$^{-/-}$ assembloids compared with controls (p value < 0.001; FDR < 0.01; Fig. 4a; Supplementary Data).

One of the ERBB4 membrane protein isoforms has a phosphotidylinositol-3 kinase (PI3K) binding site and is known to modulate the PI3K/Akt signaling pathway (Gambarotta et al., 2004; Kainulainen et al., 2000) while all isoforms can stimulate the MAPK pathway (Sundvall et al., 2008). In the transcriptomics data, differentially expressed genes were linked to the PI3K/AKT signaling pathway (*PIK3C2A, PIK3R1, PIK3R3, AKT1S1, AKT2*) and mTOR pathway (*RHEB, TSC1*). These analyses revealed that *ERBB4*$^{-/-}$ assembloids recapitulated known pathways associated with the protein in the developing human cortex (Supplementary Fig. 4b). Gene Ontology (GO) analysis found highly significant enrichment of terms for biological processes related to protein phosphorylation, regulation of actin and microtubule cytoskeleton organization, neuronal migration, dendrite morphogenesis and ER-Golgi mediated transport processes, which were all significantly downregulated (Fig. 4b-c, Supplementary Data). Similarly, significant

upregulation of calcium ion transmembrane transport, cilium assembly, cell-cell adhesion and excitatory post-synaptic potential biological processes was also observed (Fig. 4d). Importantly, knockout assembloids revealed the downregulation of genes associated with axon guidance, mTOR pathway and regulation of actin cytoskeleton pathway suggesting changes in migratory dynamics. In summary, the transcriptional landscape of *ERBB4*$^{-/-}$ assembloids agreed with our observed migratory CIN dysfunction.

At the level of diseases, common gene analysis between the differentially expressed gene data and available risk genes for intellectual disability and epilepsy showed significant overlap (ID Fold Enrichment: 0.88 and p-value: 7.92e-10; Epilepsy Fold Enrichment: 0.82 and p-value: 2.36e-08; Fig. 4d). Furthermore, the DisGeNET database through the DAVID tool linked the DEGs to intellectual disability disorder (Supplementary Data 4). The expression level of PI3K/AKT pathway genes *PIK3R1, RHEB, TSC1, AKT1S1* were validated to be downregulated using real-time quantitative PCR and RHOA/RAC pathway genes *RHOA, RAC1, CDC42, ROCK, ACTR6, ARHGAP5* were also significantly downregulated in the *ERBB4* KO assembloids (Supplementary Fig. 4c). There was no significant change observed in expression of TSC2 and PTEN. Interestingly, functional interaction of the 25 genes under neuron migration (GO:0001764) term that were downregulated in *ERBB4*$^{-/-}$ assembloids, using STRING (https://string-db.org/) highlighted a densely interconnected network of proteins centered on RHOA, NTRK2 (activator of RAC1), and FYN (Supplementary Fig. 4d, Supplementary Data 2). Thus, through a detailed analysis of transcriptional signatures from *ERBB4*$^{-/-}$ assembloids, we identified its functional impact in the dynamic expression of disease risk genes during human brain development modeling in vitro.

We took advantage of genetically engineered hiPSCs in which GAD1 was tagged with mClover fluorescent protein to generate forebrain assembloids for WT and *ERBB4*$^{-/-}$. Cell specific reporter tagging allowed for FACS based purification of GABAergic CINS from day 60 WT and *ERBB4*$^{-/-}$ assembloids to decipher the *ERBB4*$^{-/-}$ CIN protein abundance differences (Fig. 4e). Dimensionality reduction through principal-component analysis (PCA) showed distinct molecular signatures (Supplementary Fig. 4e). A total of 2050 protein groups were identified with FDR ≤ 1% in the spectral ion library. The analysis of CIN proteome revealed sufficient peptide coverage for high-confidence quantitative analysis of 1411 proteins (FDR < 0.01) with at least single unique peptides across all samples. (Supplementary Data). A more supervised approach to explore specific proteomic differences between WT and *ERBB4* KO defined 266 differentially abundant proteins (Fold change cut off = ± 1.5; p-value < 0.05). Further analysis revealed the significant differential expression of peptide fragments belonging to 134 proteins in *ERBB4*$^{-/-}$ KO CINs were upregulated and 132 proteins were downregulated (Fig. 4f).

Gene set enchichment analysis using Reactome (Gillespie et al., 2022) biological pathways on the differentially abundant proteins showed highly significant association with terms related to regulation of expression of SLITs and ROBOs, signaling by ROBO receptors, RHO GTPases activate PKNs and RHO GTPase effectors (Benjamini–Hochberg-corrected p value < = 4.58E-10 Fig. 4g; Supplementary Data 3). 42 differentially enriched proteins within the *ERBB4*$^{-/-}$ KO population were also involved in axon guidance pathways.

Discussion

ERBB4 expression is restricted to GABAergic interneurons (predominantly parvalbumin positive) in the neocortex. Whether ERBB4 affects tangential migration of interneurons directly, or whether the failure of interneurons to reach their final position in the dorsal cortex in ERBB4 pathway mutants is due to alterations in progenitor differentiation or neuronal populations has not been explored in humans. Knockout of *ERBB4* impairs, but does not completely prevent tangential migration in mice, implying that migrating neurons possess multiple, partially redundant mechanisms. Moreover, it is not understood how the loss of ERBB4 signaling alters kinetics of human CIN migration processes and which of the multiple signaling events downstream of ERBB4 have a role to play.

Fused assembloid model allowed us to investigate the way in which neurons migrate and connect up within the forebrain and displayed gross deficits in directional migration however there is a limitation of assembling organoids and imaging them live. Mechanisms such as contact inhibition and chemokine guidance aid to the directional migration of cortical interneurons in assembloids, however these mechanisms alone do not entirely explain why a CIN fails to migrate efficiently due to the possibility of other specific intrinsic mechanisms involved in facilitating cell migration. Each nucleokinetic movement of cortical interneurons is analogous to a step. Thus, average migration speed could be reduced by lowering step frequency and/or step distance. To assess such kinetic features, we developed a system that supports nanofiber-guided migration from VFOs. The ventral patterning protocol used in this study, unlike other sub-pallial models, allows the establishment of all zones of the ganglionic eminence (medial, lateral and caudal), thereby covering the high diversity of GABAergic interneurons derived from each of the zones (Bagley et al., 2017).

In contrast to radial migration of bipolar CINs where radial glia cells act as a scaffold for migration, the physical scaffold for their tangential migration is not well established (Martinez-Martinez et al., 2019; Tanaka et al., 2009). In the developing human brain, the ECM constitutes roughly 40% of the brain volume (Jovanov Milosevic et al., 2014; Sykova & Nicholson, 2008) and defines the mechanical environment of these migrating neurons. Mechanosensation driven by the interplay between such ECM biophysical cues and intracellular signaling are therefore major players in tangential migration. Therefore, we chose different arrays of aligned nanonets to mimic the micro-fibrillary environment and investigated the migration of interneurons (GAD67-mClover + cells) from ventral forebrain organoid. Individual fiber diameters of nano-fibrous scaffolds can approach that of physiological collagen fiber bundles, between 50 and 500 nm (Siadat et al., 2021). Migration assay on these nanofibers is different from those on classical flat surfaces as 2D substrates are stiffer than the *in vivo* ECM.

The average motility rate of interneurons reported in mice *in vivo* imaging studies and in organotypic slice cultures is 40–50 μm/hr (Inada et al., 2011; Nichols et al., 2008; Tsai et al., 2007). This is in concordance with the observed average migration rate of WT and *ERBB4*$^{-/-}$ CINs on scaffolds emphasizing the significance of this system. In *ERBB4*$^{-/-}$ we observed unidirectional collective migration as compared to efficient separate migration of wildtype interneurons. For WT CINs on scaffolds the leading process

oriented in all directions while cells also exhibit fiber switching and sudden changes in direction of motion. This is in agreement with reports from mice cortex preparations and this random walk migration behaviour reportedly helps interneurons to disperse throughout the cortex (Tanaka et al., 2009; Yanagida et al., 2012; Yokota et al., 2007). We also observed processes resembling long distance extending axons (Supplementary Movie 10).

The native ECM of tissues is composed of protein fibers with varying diameter and stiffness and cells are known to move through the interstitial matrix by extensive active local rearrangement of the ECM fibers *in vivo* (van Helvert & Friedl, 2016). In our nanofiber migration setup, we observed cells applying contractile forces as visualized by the deflection of the fibers resulting in their remodeling (Supplementary movie 11). Few lines of evidence from mice models report interneurons and neuroblasts (neuronal precursors) to be closely associated with vascular networks and their leading process has been shown to wrap around blood capillary during this migration while adhesion to radial glia cells is reported in case of radial migration upon reaching the dorsal cortex (Won et al., 2013)(Won 2013). Upon using parallel orientation nano-fibers we could observe unidirectional helical locomotion of interneurons (Supplementary Fig. 3o). Therefore, nanofiber platform can accelerate migration studies and facilitate quantitative screening of different modes of neuronal migration and its kinetics for future pharmacological and genetic studies.

In previous mouse studies, interneurons with altered ERBB4/PI3-kinase activity are shown to escape the MGE/LGE corridor, but their migration is random, the leading process anomalous, and many cannot traverse out of the pallial/sub-pallial border to reach the dorsal cortex. While in the event of complete loss of ERBB4/NRG1 signaling in the developing forebrain, a proportion of interneurons stay confined to the MGE (Flames et al., 2004; Rakic et al., 2015). Also, the inactivation of kinase activity of ERBB4 or its genetic ablation in postmitotic interneurons does not impair their migration into the cortex (Fazzari et al., 2010; Luo et al., 2021). Therefore, distinct ERBB4 modulated pathways might be required for tangential interneuron migration through the developing forebrain.

In a recent study, ERBB4 knockdown in ventral thalamic organoids showed prolonged reduced neuronal activity with decreased average amplitude and frequency due to dysregulation of small conductance calcium-activated K + channels (Kiral et al., 2023). Interestingly, the upregulation of 22 genes related to the calcium ion transmembrane transport biological process was observed and increased expression of KCNN2 gene that encodes for SK2 channels was seen in the *ERBB4* KO organoids which has been reported to cause diminished bursting and impaired neuronal activity (Cueni et al., 2008). CINs form inhibitory synapses onto excitatory pyramidal neurons (PyNs) and control their activity by releasing GABA. ERBB4 receptor not only subcellularly localizes to the inhibitory synapses of GABAergic INs but has also been implicated in the formation and maturation of postsynaptic sites of excitatory synapses onto CINs (Del Pino et al., 2013; Fazzari et al., 2010). Batista-Brito et al. reported that early deletion of ERBB4 causes elevated firing of cortical interneurons and excitatory neurons (Batista-Brito et al., 2023). ERBB4 therefore regulates excitatory synaptic input to pyramidal neurons and ERBB4-LOF from PV-INs leads to loss of dendritic spines and dysregulation of excitatory pyramidal neuron dendritic architecture in hippocampal pyramidal neurons and some prefrontal cortical neurons (Barros et al., 2009). In line with

these experimental observations, our pathway analysis revealed an upregulation in genes involved in excitatory postsynaptic potential, highlighting synaptic alterations in the ERBB4 knockouts and downregulation of dendrite morphogenesis-associated genes. As a result of ERBB4 disruption, this hyperactivity neurons could be possible through a compensatory mechanism in order to maintain excitation/inhibition balance. Future studies should screen for the detailed effects on circuit assembly and cell activity of *ERBB4* KO mature interneurons post-migration.

The Slit Guidance Ligand proteins (SLITs) are large diffusible ligands for Robo (Roundabout) transmembrane receptors that are expressed by cells in the neocortex (Andrews et al., 2006) and are reported to guide migrating neurons and their axon extensions in the CNS through chemorepulsion (Andrews et al., 2006; Marin et al., 2003). SLIT1-ROBO1 signaling has been shown to repel mouse GABAergic CINs derived from the GEs thereby guiding them towards the cortex (Andrews et al., 2006). CINs reportedly migrate along a dynamic gradient of SLIT1 with higher expression in the ventral region and lower towards the dorsal telecephalon, complementary to ROBO1 spatial expression pattern (Andrews et al., 2008). Therefore, downregulated SLIT1 protein in CINs could be a possible interpretation for less tendency of CINs to migrate away from VFOs. The in *vivo* ventricular specific expression of SLIT1 during the period of CIN migration to the cortex (Bagri et al., 2002) also suggests its strong role in directional CIN migration however, interestingly, in mice Slit1, Slit2 double mutants, tangential migration is not perturbed (Marin et al., 2003). Strikingly upon looking back in our *ERBB4*$^{-/-}$ KO transcriptome data, we also found ROBO1 (receptor for SLIT1) to be highly significantly downregulated (lg2fc: -8.68028 and p value: 4.04E-05) and as suggested by literature ROBO1 signaling can play a role in CIN migration independent of SLIT1 (Marin et al., 2003). Rho GTPase activating proteins (GAPs) are also important downstream interactors of ROBO1, transducing the signal for actin polymerization by inactivation of CDC42 or activation of RHOA and RAC1 (Wong et al., 2001). Notably, FYN kinase is also known to regulate RHO GTPases and thereby cell migration (Liang et al., 2004; Yeo et al., 2011). In mice oligodendrocyte precursor cells, it has been reported that Slit2 can mediate repulsive migratory effects through FYN/RHOA signaling in vitro through a direct inactivation of FYN kinase by ROBO1 (Liu et al., 2012). Although a direct relation of ERBB4 with these proteins is not clear or fully elucidated from literature, our omics data identifies and links interesting potential candidates like FYN, SLIT1 and ROBO1 for further investigation for their role in the migratory signaling cascade perturbed in *ERBB4*$^{-/-}$.

Limitations of this study

Our study utilized ventral organoid modeling protocol that resembles all zones of ganglionic eminences (medial, lateral and caudal) considering the high diversity of GABAergic interneurons derived from each of the zones and can be used to decipher interneuron subtype-specific effects of *ERBB4* which have not been covered in this study. Inherent limitations of the system include the lack of immune cells and vascularization. Also, *in vivo* there are other non-neuronal cells that actively participate in interneuron generation and migration, such as vascular endothelial cells and oligodendrocyte precursors (Lepiemme et al., 2022). The current organoid on scaffold platform does not capture those cell-cell interaction effects

on tangential migration. There is a lack of biochemical gradients that also potentially impacts migration dynamics in vivo. In future studies, we aim to include these interactions by incorporating dorsal lineage cells in the vicinity of interneurons for gradients of soluble guidance cues in the form of chemokines that encourage the directional migration of interneurons.

Materials and Methods

iPS cell culture

Pluripotent stem cell lines were cultured in feeder-free conditions on Geltrex™ LDEV-Free Reduced Growth Factor Basement Membrane Matrix (Gibco) or Matrigel (Corning Matrigel hESC-Qualified Matrix, LDEV-free, Cat. No. 354277) coated cell culture dishes containing Essential 8 medium (ThermoFisher Scientific) with supplements and 1X Pen-Strep (ThermoFisher Scientific), at 37°C in 5% CO2. Media change was done after every 24 hrs. Upon attaining ~ 80% confluency cells were sub-cultured (split 1:6) using enzyme free passaging reagent, ReLeSR™ (STEMCELL Technologies) according to product manual, alternatively 0.5 mM EDTA in sterile DPBS without calcium and magnesium was used for passaging. hiPS cell lines were maintained below passage 50, were negative for mycoplasma (assayed with MycoAlert PLUS Mycoplasma Detection Kit, Lonza) and karyotypically normal (hPSC Genetic Analysis Kit, STEM CELL Technologies). The IMR90 hiPSC line was authenticated using STR analysis completed in CSIR-IGIB (in 2023). Genetic profiling was performed for cell line authentication using GenePrint® 10 System. The amplified products were subjected to capillary electrophoresis on 3500xL Genetic Analyzer (Applied Biosystems) and data was analyzed by GeneMapper 5 software.

CRISPR guide RNA design

The CRISPR guide RNAs for ERBB4 and GAD1 targets were designed using the CRISPOR web tool13. The guides were designed to maximize on-target efficiency and minimize off-target sites in intragenic regions. For GAD1, a guide was designed to target the C-terminal domain to knock-in a fluorescent reporter and selection construct before stop codon (GAD1 gRNA targeting sequence: 5'-CGAAGGATGATTACAGATCC – 3'). The ERBB4 targeting guides were designed to delete the exon 2 resulting in a stop codon immediately in coding frame to knockout the protein [ERBB4 gRNA1 with PAM: 5'-ATATTTCGATCGTCATTAAG – 3' (AGG); ERBB4 gRNA2 with PAM: 5'-AGAGATAGCGAAACGCACCC – 3'(AGG)].

Plasmids and Cloning

gRNA sequence targeting the AAVS1 intron 1 was cloned in PX458-3xHA-FnCas9 (Addgene #130969) plasmid using BbsI restriction enzyme based cloning strategy (Ran et al. 2013). For delivery of only gRNA in iCas9 IMR90, dual guide RNA delivery vector with GFP reporter was constructed by inverse PCR of dual sgRNA (BbsI-BsaI) vector in the lab. crRNAs were cloned in this vector for GAD1 and ERBB4 targeting and confirmed with sanger sequencing. Primer sequences for crRNA cloning and vector generation are provided in the supplementary materials (Supplementary Data 1).

CRISPR/Cas9 mediated genomic knock-in of iCas9

pAAVS1-TRE-Cas9-puro-polyA-CAG-rtTA (Addgene #107270) plasmid has a single donor cassette containing both the rTetR activator under CAG promoter and the Tetracycline Response Element (TRE) promoter driving the expression of Cas9 with homology arms targeted to the AAVS1 locus. gRNA sequence targeting the AAVS1 intron 1 (5'-GGGGCCACTAGGGACAGGAT-3') was cloned in PX458-3xHA-FnCas9 (Addgene #130969) plasmid using BbsI restriction enzyme based cloning strategy14 and colonies post-transformation screened for successful gRNA sequence incorporation under U6 promoter. DNA oligo sequences for crRNA cloning and vector generation are provided in the Table S1. 1 hour before electroporation iPSCs were treated with 10 µm ROCK inhibitor (Y-27632). 70%-80% confluent iPSC colonies were harvested using StemPro™ Accutase™ Cell Dissociation Reagent (ThermoFisher Scientific Cat. No. A1110501) and pipetted to make single cell suspension. For electroporation, 12ug of PX458-3xHA-FnCas9 (plasmid with gRNA) and 6ug of linearized donor plasmid were added to Resuspension Buffer R with final volume of 100ul. 6 x 105 cells were resuspended in the 100 µL of R buffer + plasmid mix and electroporation was performed using Neon® Transfection System 100 µL tip (ThermoFisher Scientific Cat. No. MPK1025) with a single pulse at 1400 V, 30 milliseconds pulse width. The electroporated cells were transferred immediately to a Matrigel coated 6-well plate containing 2 ml of Essential 8 media with 10 µM ROCK Inhibitor and incubated at 37°C and 5% CO2. After 12 hours cells were washed with DPBS and re-incubated with fresh medium. 48 hours post electroporation, cells were selected with 1ug/ml puromycin (MP biomedicals) for 3 days. Further dose was increased to 3ug/ml and cells were maintained in selection for a week. Selected clones were picked and two clones were expanded further, followed by gDNA extraction by Wizard® Genomic DNA Purification Kit (Promega Corporation, Cat. No. A1120) following the manufacturer's instructions and PCR genotyping was done using primers mentioned in supplementary materials.

Fluorescent Reporter tagging in hiPSCs

For labeling CINs in culture, GAD1 gene was targeted in the iCas9 IMR90 hiPSCs for which pUC57 donor construct with P2A-mClover and Hygromycin selection marker under PGK promoter with 800bp flanking homology arms was synthesized. hiPS Cells were treated with doxycycline (2 µg/ml) one day before electroporation of plasmid vector for gRNA and donor DNA. 72 hours post electroporation, GFP positive cells per sample were sorted using BD FACS Melody Cell Sorter (BD Biosciences-US) and re-plated for further selection in Hygromycin antibiotic (150 µg/ml). Genotypic PCR was performed from the gDNA isolated from 7 clones and two were confirmed by sanger sequencing of the PCR amplicons.

ERBB4 knockout generation and genotyping

For dual guide targeting of ERBB4 gene, GFP positive cells were bulk sorted and re-plated in CloneR (Stem Cell technologies, Catalog #05888) supplemented media for further colony picking and PCR screening. For genotyping by PCR to verify the deletion, few bulk sorted cells were lysed to isolate gDNA. Genomic DNA for genotyping was extracted by Wizard® Genomic DNA Purification Kit (Promega Corporation, Cat. No. A1120) following the manufacturer's instructions. Taq Polymerase based PCR amplification of was done with primers listed in Table S1, to verify the deletion of exon 2 in the ERBB4 gene. The expected PCR products are: 628 bp for exon 2 containing (wild-type) and 192 bp for exon 2 deleted (ERBB4 KO).

Monolayer GABAergic neuron differentiation from hiPSCs

Differentiation of hiPSCs to GABAergic interneurons was done as per published protocols for CIN generation15, 16. ~80% confluent hiPSCs were detached with Gentle Dissociation Medium (Stem Cell Technologies) and grown as floating spheres in low-adherent cultureware in KSR media (DMEM, 15% knockout serum replacement, 2 mM L-glutamine and 10 μM β-mercaptoethanol (Invitrogen). 10 μM Y27632 was added to the culture on the first day of differentiation again to prevent single cell-induced cell death of iPSCs. SMAD signaling inhibitors, 1uM Dorsomorphin for BMP and 10uM SB43542 for TGF-β, were added for neuralization. For neuroectoderm induction after 4 days, cells were treated with neural induction medium with NEAA, 5 ml of N-2 supplement and heparin. On day 7, EBs were plated on Laminin (Sigma) coated plates for attachment and fed the culture with the same medium every other day until day 10 till neural rosettes appear. For patterning neuroepithelia to MGE progenitors, NIM containing 1.5 μM Purmorphamine (Peprotech) was added every other day. Around day 25, neural differentiation was started with neurobasal media supplemented with N2 supplement, Non-Essential Amino Acids and trophic factors: 1 μM cAMP (cyclic AMP),10 ng/ml BDNF (Brain Derived Neurotrophic Factor), 10 ng/ml GDNF (Glial cell line-derived neurotrophic factor), 10 ng/ml IGF1 (Insulin-like Growth Factor 1) for neuron survival and maturation. At day 40 of differentiation, CINs were trypsinized and then plated on polyornithine (PLO; 15 mg/ml; Sigma) and Laminin (1 mg/ml; Sigma)-coated plates in DMEM/F12 media with B27 supplement (1:100, Invitrogen) and trophic factors. Cells were fixed for immunocytochemistry at the 6th week of differentiation and also harvested for RNA preparation.

qRT-PCR

2 clones of iCas9_IMR90 iPSCs were treated with doxycycline (2 mg/ml) for 72 hrs and analyzed for Cas9 expression by qPCR. RNA was extracted using TRIzol. cDNA synthesis was performed using 500ng of total RNA and the QuantiTect Reverse Transcriptase enzyme kit (Qiagen) according to the manufacturer protocols. qPCR reactions were performed using SYBR Green master mix (Takara) on a Roche 384-well machine using the following reaction protocol: 1) 95°C for 3min, 2) 95°C for 10s, 3) 60°C for 10s, 4) 72°C for 30s, 5) go to 2, 40 cycles, 6) 95°C for 1min, 7) 50°C for 10s. Quantification was performed in excel by calculating the ΔCt value using TBP or GAPDH as a reference gene. Data is presented as expression level (2-ΔΔCt) relative to un-transfected control IMR90_IPS cells.

Immunostaining and microscopy

For 2D monolayer immunostaining experiments, cells plated on coverslips were first washed with 1x PBS then fixed with 4% paraformaldehyde for 15 minutes at room temperature. Cells were then washed 3x with PBS and permeabilized with 0.25% Triton X-100 and blocked for 1 hour with 3% BSA in 0.1% PBS-Tween for 1hr. Cells were then incubated with primary antibody diluted in 1% BSA in 0.1% PBS-Tween overnight at 4-degree C. Cells were washed 3 times with 0.1% Tween 20 in PBS and incubated with secondary antibodies. Coverslips were then mounted on glass slides using ProLong™ Diamond Antifade mountant with DAPI (Invitrogen, P369366). The list of the primary and secondary antibodies and dilution used is mentioned in supplementary table (Table S2). Confocal microscopy system (Leica SP8) with 63X

objective and widefield fluorescence microscope, EVOS FL Auto imaging system (ThermoFisher Scientific) were used for visualizing the slides.

Western Blotting

Western blot experiment was performed to analyze change in ERBB4 protein expression upon knockout. The hiPS cells were lysed using RIPA lysis buffer (ThermoFisher, Pierce™) to prepare the cell lysate. 70 µl of the lysis buffer was added to pelleted cells from a well of 6-well plate along with 1×Protease Inhibitor Cocktail (PIC, Roche). The cells were then vortexed in the mix and incubated at 4°C for 1hr. Protein lysate from each sample was collected and the concentration of the protein was estimated using Pierce™ BCA Protein Assay Kit (ThermoFisher). For each sample, 30 µg of protein was loaded into the wells of 10% SDS gel and PAGE was performed using SDS running buffer (2.5mM Tris base, 19mM Glycine, 0.1% SDS in autoclaved milliQ). The proteins were then transferred from the gel to the PVDF membrane (GE Healthcare Life-Science) in Bio-Rad vertical gel Transfer Apparatus using Transfer buffer (2.5mM Tris base, 19mM Glycine, 20% v/v Methanol in autoclaved milliQ) at 4°C for 1.5 hrs at 95 V. After the transfer was complete, the membrane was cut according to the required protein size and kept for blocking with 5% BSA in 1×TBST (20mM Tris base, 150 mM NaCl and 0.2% Tween-20) on a rocker at room temperature for 2 hrs. After blocking, the blots were incubated with Recombinant Anti-ErbB4 / HER4 antibody (Abcam, Cat. No. ab109273) at 1:1000 dilution on a rocker at 4°C overnight. Beta-Tubulin antibody (Abcam, Cat. No. ab6046, 1:5000 dilution) was taken as the loading control. After primary antibody incubation, the blots were washed three times for 10 min each with 0.2% TBST. Post washing, the same blots were incubated with a secondary Goat Anti-rabbit IgG (HRP) antibody at 1/10,000 dilution on a rocker for 2 hrs at room temperature. Post secondary antibody incubation, the blots were washed three times for 15 mins each. For signal development, EMD Millipore™ Immobilon Western Chemiluminescent HRP Substrate (ECL) was used to develop the blots in Gel Doc instrument (Syngene).

Fused forebrain assembloid culture

Cerebral organoids and fusions (assembloids) were generated using previously published protocols with few modifications5, 7. Briefly, iPS cells at around 70–80% confluency were treated with 1× Accutase solution (StemPro Accutase Cell Dissociation Reagent,Gibco, Cat. No.: A1110501) for 10 min at 37°C and 9000 cells per well of a 96-well ultra-low attachment U-bottom plate (Corning, Cat. No.7007) were seeded in 150 µL Essential 8 medium supplemented with 10 µM Rock Inhibitor. For 50ml of neural induction media, 0.5ml N2 supplement (Invitrogen, cat. no. 17502048), 0.5ml GlutaMAX (Invitrogen, cat. no. 35050-038), 0.5ml Minimal essential medium non-essential amino acids (MEM-NEAA, 100X Gibco, cat no. 11140050) and 500µl Heparin (Sigma) solution (1 mg/ml solution made in PBS) were added to 50ml DMEM/F12. For induction of dorsal forebrain, neural induction medium was supplemented with 0.5 µM CyclopamineA (CycA, Calbiochem, cat. no. 239803) and for ventral forebrain, media was supplemented with 100 nM SAG (Smoothened Agonist, Merck-Millipore, Cat. No. US1566660) and 2.5 µM IWP2 (Inhibitor of WNT pathway, Sigma, cat. no. I0536). For 50ml of differentiation media: 25ml DMEM/F12 media, 25ml Neurobasal media, 250 µl N2 supplement, 500 µl of B27 supplement (with or without vitamin A supplement), 12.5µl Insulin solution, 17.5µl of a 1:100 solution of 2-ME (in DMEM/F12), 5ml Glutamax,

2.5ml MEM-NEAA and 5ml of Penicillin + Streptomycin solution were mixed and sterile filtered using a 22µm syringe filter. Dorsal and Ventral EBs were embedded together in Matrigel (Corning, cat. #3524234) droplet on day 12 in differentiation media without vitamin A and then transferred to an orbital shaker at 70 rpm in low attachment dishes on day 16. From day 16, organoids were fed with organoid differentiation media having vitamin A every 3–4 days.

Immunohistochemical analysis of Organoids

Organoid samples were prepared as previously described5. At the time point of choice, organoids were transferred to a 6-well plate by gently pipetting with a cut 1 ml pipette tip and fixed in 4% PFA (Paraformaldehyde) for 30 minutes at room temperature and after PBS washes, incubated overnight at 4°C in 30% sucrose solution. Organoids were then embedded in gelatin/sucrose solution and left to polymerize for 30 minutes. Using a scalpel blade, small blocks were cut out containing the organoids and snap freezing was done via immersion into a chilled isopentane (Merck, Cat. No. PHR166) bath. Blocks were then stored in -80. For cryosectioning, blocks were embedded in Tissue Freezing Medium (Leica Biosystems) and sectioned at 15–20 µm with a cryostat (Leica) onto glass slides (Fisherbrand Superfrost Plus Microscope Slides) using standard techniques. For immunostaining, slides were washed with PBS once to remove tissue freezing medium and sucrose. A hydrophobic PAP pen (Super Pap Pen, Cat. 8899, ThermoFisher Scientific) was used to draw a circle around sections for adding solutions. Blocking was performed for 1 hour at RT with 10% Normal Goat Serum (NGS), 0.3% Triton-X in PBS. Primary antibodies diluted in 5% NDS, 0.3% Triton-X in PBS solution were added and incubation done in a humidified chamber at 4°C overnight. After three PBS washes, appropriate secondary antibodies were added for 2 hours at RT. A list of the primary and secondary antibodies is provided in the Table S2. Slides were then washed thrice with PBS and DAPI (0.1mg/ml) solution added before mounting using Antifade mountant (Invitrogen, P369366) on the sections and placing a coverslip on top.

Microscopy and organoid size analysis

Brightfield images of organoids during culture were taken using EVOS Auto FL microscope (Invitrogen) and EVOS M5000 imaging system (Invitrogen). Area values were obtained by tracing the outline of individual organoids on ImageJ, which measured area pixels. Measurements were plotted for control and KO organoids of each experimental batch.

2D coverslip neuron outgrowth assay

ERBB4 KO and control iPSC-derived ventral forebrain organoids (40 day onwards) were dissociated gently by pipetting into visible spheres and plated on 15mm coverslips coated with Poly-L-Ornithine (100ug/mL, Sigma-Aldrich P3655- 100MG) and Laminin (50ug/mL, Sigma-Aldrich L2020-1MG) and organoid differentiation media was added. Organoids were allowed to adhere to the surface and after 48 hours media was changed. Brightfield and GFP channel images were acquired on the next 2 days post attachment to quantify the outgrowth of interneurons from KO and WT organoid surface for which radial distance from periphery or boundary of organoids was calculated from ImageJ. For timelapse imaging,

frames after every 10 minutes were taken at 10x or 20x magnification on the EVOS FL Auto imaging system (ThermoFisher Scientific) with environmental chamber setup.

Dissociation of organoids on nanofiber scaffolds for imaging

Nanofiber scaffolds were placed on glass coverslip bottom µ-Dish (Ibidi) upon applying vacuum grease (Dow Corning High Vacuum Grease, Sigma) on the edge and washed twice with ethanol and dried to make sterile. Coating of PLO-Laminin or 3% Matrigel was done on scaffold. Organoids were dissociated by pipetting up and down with a slightly cut tip of P1000 to break into smaller visible clumps before plating on scaffolds gently without touching or disturbing the suspended fibers from pipette tip. Neural differentiation medium was added from the edge without letting organoids float away from the fibers and the dishes were incubated at 37 degrees for 12 hrs. Post-attachment, media was added to cover the scaffolds completely and long term live imaging was performed after 3 days of seeding with phase contrast images taken at 3 or 5 minute intervals for more than 16 hrs. Live imaging was done on a widefield EVOS FL Auto imaging system and EVOS M5000 (ThermoFisher Scientific) system with EVOS onstage incubator (Cat. No. AMC1000). ImageJ was used for analysis.

Migration parameter quantification

ImageJ was used for the post-acquisition analysis of cell mobility. To estimate the length of individual saltations, interneurons displaying a swelling of the soma were identified, and distance (in µm) to the new position of the soma following nucleokinesis was recorded. The time necessary for this movement was used to calculate the speed when mobile. To estimate directness of movement, the x and y coordinates of each cell per frame and time were extracted with the Manual Tracking plugin (ImageJ) and was used to calculate the Euclidian (E) distances traveled per cell over time. Videos were processed using ImageJ.

Bulk RNA sequencing and differential expression analysis

RNA purification, quantification, and quality check: Fused forebrain assembloids at day 60 (four random samples from each individual batch of WT and ERBB4 KO at the same time point) were collected and total RNA was purified using the RNeasy Mini Kit (Qiagen) with DNase I digestion following the manufacturer's protocol. RNA quality was checked on a Bioanalyzer instrument (Agilent Technologies) using an RNA 6000 Pico Chip. Only RNA samples with RNA integrity number (RIN) values > 7.4 were used for library preparation and sequencing. Four biological replicates were analyzed for each group. The Illumina NovaSeq6000 platform was used for sequencing in the 150 nt, paired-end configuration to yield approximately 40 million mapped reads per sample.

Quality control and differential gene expression analysis: The RNA-seq analysis consisted of quality control, trimming, alignment, quantification, and differential gene expression analysis. It was conducted using a variety of computational tools, with versions specified to ensure reproducibility. Quality control on paired-end raw sequence reads was done using FastQC v0.11. Approximately 43 million paired-end reads

per sample, obtained from both wild type and ERBB4 KO groups consisting of 4 biological replicates, resulted in a total of 16 fasta files. Trimmomatic v0.3917 was utilized for adapter removal and quality trimming. FastQC was again applied to verify the improvement in read quality. MultiQC v1.1418 was used to aggregate the FastQC reports for a comprehensive overview of the data quality before and after trimming. For read alignment, Kallisto v0.44.019 was employed, aligning the reads to the human genome (GRCh38). Subsequently, transcript abundance was quantified with Kallisto. The transcript-level counts were converted into gene-level counts using the tximport R package v1.24.020 in R v4.2.2. Differential gene expression analysis between WT and ERBB4 KO samples was performed using the DESeq2 R package v1.36.021 and results were visualized as volcano plot using EnhancedVolcano v1.14.0 (https://github.com/kevinblighe/EnhancedVolcano). After identifying significant differentially expressed genes (DEGs) using a stringent cut-off of absolute log2 fold change > 1 and false discovery rate (FDR) < 0.05, DEGs were further subjected to functional enrichment and pathway analysis for which the Database for Annotation, Visualization, and Integrated Discovery (DAVID v6.8)22, 23 was used to perform Gene Ontology (GO) analysis. Pathway analysis was done using Kyoto Encyclopedia of Genes and Genomes (KEGG) within DAVID tool to identify the enriched pathways in our DEGs24. The DisGeNET database through DAVID enabled the identification of DEGs associated with diseases.

Enrichment analysis: A list of highly confident Intellectual disability associated genes were retrieved from the SysID database (https://www.sysid.dbmr.unibe.ch)25 with 1500 primary ID genes, causing 1797 ID related disorders, and 1248 ID candidate genes and 1215 genes from the Epilepsy Gene-Disease Association list (C0014544) from https://www.disgenet.org/search. To identify which of these human genes overlap with the list of DEGs in ERBB4 KO assembloids, fold enrichment was calculated by comparing the proportion of overlapping genes to the expected chance of finding an ID/epilepsy disease gene in the human coding genome. The statistical significance of the overlap was determined using a two-sided Fisher’s exact test.

Proteomics and analysis

Sample preparation: Proteomic studies were performed on the WT and ERBB4 KO cortical interneurons in four biological replicates. Tissue samples were lysed in RIPA with a protease inhibitor cocktail and centrifuged at 15000 g for 15 minutes at 4°C. The supernatant was collected in a fresh microcentrifuge tube and processed for proteomics analysis. Protein precipitation from these samples was performed by overnight incubation with pre-chilled acetone followed by centrifugation at 15000g for 15 minutes at 4°C. The protein pellets were suspended in 0.1M Tris-HCl with 8 M urea, pH 8.5. Protein quantitation was performed using the Bradford assay. 20 µg of protein from each sample was processed for quantitative proteomics analysis (SWATH-MS) and 300µg protein, pooled from all the samples from WT and ERBB4 KO organoid samples were utilized for the generation of spectral ion library. The protein samples were reduced by the addition of 2mM final concentration of dithiothreitol (DTT) and heating at 56℃ for 30 minutes. Samples were then cooled down at room temperature and alkylated using 2.2 mM final concentration of iodoacetamide (IAA) and incubation in the dark, at room temperature for 20 minutes. Samples were then diluted with 0.1 M Tris-HCl buffer, pH 8.5, to bring urea concentration in the sample

below 1M concentration. These samples were then subjected to trypsin (V5111, Promega) digestion in an enzyme-to-substrate ratio of 1:20 (trypsin: protein) for 16 hours at 37 ℃. The tryptic peptides were cleaned up using Oasis HLB 1 cc Vac cartridges (Waters) using the manufacturer's protocol, vacuum dried in a vacuum concentrator, and stored at -20℃ till LC-MS/MS analysis. The protein digest pool for spectral library generation was fractionated into 8 fractions using a hand-held cation exchange cartridge (part no. 4326695, SCIEX) and using an increasing concentration of ammonium formate buffer (35 mM-350 mM ammonium formate, 30% v/v ACN, and 0.1% formic acid; pH = 2.9). Peptides from each of these fractions were cleaned up using C18 ZipTip (Millipore, USA) and analyzed on the mass spectrometer.

Data acquisition: Spectral ion library generation: Each fraction was then analyzed on a quadrupole-TOF hybrid mass spectrometer (TripleTOF 6600, SCIEX) coupled to an Eksigent NanoLC-425 system in data-dependent acquisition (DDA) mode. Optimized source parameters were used, curtain gas and nebulizer gas were maintained at 25 psi and 20 psi respectively, the ion spray voltage was set to 5.5 kV, and the temperature was set to 250°C. About 4 µg of peptides were loaded on a trap column (ChromXP C18CL 5 µm 120 Å, Eksigent, SCIEX) and online desalting was performed with a flow rate of 10 µl per minute for 10 min. Peptides were separated on a reverse-phase C18 analytical column (ChromXP C18, 3 µm 120 Å, Eksigent, SCIEX) in an 87-minute-long buffer gradient with a flow rate of 5 µl/minute using water with 0.1% formic acid (buffer A) and acetonitrile with 0.1% formic acid (buffer B) as follows:

Time (min)	% A	% B
0	97	3
68	75	25
73	65	35
75	20	80
78	20	80
79	97	3
87	97	3

Data was acquired using Analyst TF 1.7.1 Software (SCIEX). A 1.8-sec instrument cycle was repeated in high sensitivity mode throughout the entire gradient, consisting of a full scan MS spectrum (400–1250 m/z) with an accumulated time of 0.25s, followed by 30 MS/MS experiments (100–1500 m/z) with 50 msec accumulation time each, on MS precursors with charge state 2 + to 5 + exceeding a 150-cps threshold. Rolling collision energy was used and the former target ions were excluded for 15 seconds.

SWATH-MS data acquisition: Quantitative analysis of proteome from the WT and ERBB4 KO samples was performed using the Sequential Window Acquisition of All Theoretical Mass Spectra (SWATH-MS)

method by operating the mass spectrometer in data-independent acquisition mode using optimized parameters. The tryptic digests from the samples were suspended in 0.1% formic acid and analyzed in SWATH-MS mode on the same instrument with similar LC gradient and source parameters as DDA runs. A SWATH-MS method was created with 100 precursor isolation windows, defined based on precursor m/z frequencies in DDA run using the SWATH Variable Window Calculator (SCIEX), with a minimum window of 5 m/z. Accumulation time was set to 250 msec for the MS scan (400–1250 m/z) and 25 msec for the MS/MS scans (100–1500 m/z). Rolling collision energies were applied for each window based on the m/z range of each SWATH and a charge 2 + ion, with a collision energy spread of 5. The total cycle time was 2.6 seconds. Four biological replicates per group were analyzed and a pooled quality check (QC) sample was injected after every 4 samples to check technical variation.

Data analysis: A merged database search for DDA runs was performed using ProteinPilotTM Software 5.0 (SCIEX) against Homo sapiens proteome from UniProtKB (UP000005640, 104451 entries, accessed in July, 2023). The Paragon algorithm was used to get protein group identities. The search parameters were set as follows: sample type- identification, cysteine alkylation-iodoacetamide, and digestion- trypsin. The biological modification was enabled in ID focus. The search effort was set to 'Thorough ID' and the detected protein threshold [Unused ProtScore (Conf)] was set to > 0.05 (10.0%). False discovery rate (FDR) analysis was enabled. Only proteins identified with 1% global FDR were considered true identification. The search result file from ProteinPilotTM Software was used as a spectral ion library for SWATH analysis. Peak areas for proteins from SWATH analysis were extracted using SWATH 2.0 microapp in PeakView 2.2 software (SCIEX), and shared peptides were excluded. SWATH run files were added and retention time calibration was performed using peptides from abundant proteins. The processing settings for peak extraction were: a maximum of 10 peptides per protein, 5 transitions per peptide, > 95% peptide confidence threshold, and 1% peptide FDR. XIC extraction window was set to 5 min with 50 ppm XIC Width. All information was exported in the form of MarkerView (.mrkvw) files. In MarkerView 1.2.1 (SCIEX), protein area data was normalized, the data normalization strategy used was total area sum normalization and further statistical analysis was performed in MetaboAnalyst 5.0 (PMID: 34019663). A cut-off of 1.5-fold change was set for identifying differentially expressed proteins. Pathway enrichment analysis was performed in DAVID bioinformatics resources (PMID: 19131956, 35325185).

Significance tests

Individual organoids were treated as biological replicates, unless otherwise indicated in the Figure Legends. Data are presented as mean ± S.E.M. or mean + S.D., unless otherwise indicated in the Figure Legends. Statistical analyses were performed using the Student's t-test in GraphPad Prism v.8.0 software. Significance was defined by p-value < 0.05. Organoid samples were randomly taken from the culture for experiments and analysis. Other statistical details of experiments can be found in the Figure Legends.

References

1. Acharya, S., Mishra, A., Paul, D., Ansari, A. H., Azhar, M., Kumar, M., Rauthan, R., Sharma, N., Aich, M., Sinha, D., Sharma, S., Jain, S., Ray, A., Jain, S., Ramalingam, S., Maiti, S., & Chakraborty, D. (2019). Francisella novicida Cas9 interrogates genomic DNA with very high specificity and can be used for mammalian genome editing. *Proc Natl Acad Sci U S A*, *116*(42), 20959-20968. https://doi.org/10.1073/pnas.1818461116
2. Andersen, J., Revah, O., Miura, Y., Thom, N., Amin, N. D., Kelley, K. W., Singh, M., Chen, X., Thete, M. V., Walczak, E. M., Vogel, H., Fan, H. C., & Pasca, S. P. (2020). Generation of Functional Human 3D Cortico-Motor Assembloids. *Cell*, *183*(7), 1913-1929 e1926. https://doi.org/10.1016/j.cell.2020.11.017
3. Andrews, W., Barber, M., Hernadez-Miranda, L. R., Xian, J., Rakic, S., Sundaresan, V., Rabbitts, T. H., Pannell, R., Rabbitts, P., Thompson, H., Erskine, L., Murakami, F., & Parnavelas, J. G. (2008). The role of Slit-Robo signaling in the generation, migration and morphological differentiation of cortical interneurons. *Dev Biol*, *313*(2), 648-658. https://doi.org/10.1016/j.ydbio.2007.10.052
4. Andrews, W., Liapi, A., Plachez, C., Camurri, L., Zhang, J., Mori, S., Murakami, F., Parnavelas, J. G., Sundaresan, V., & Richards, L. J. (2006). Robo1 regulates the development of major axon tracts and interneuron migration in the forebrain. *Development*, *133*(11), 2243-2252. https://doi.org/10.1242/dev.02379
5. Bagley, J. A., Reumann, D., Bian, S., Levi-Strauss, J., & Knoblich, J. A. (2017). Fused cerebral organoids model interactions between brain regions. *Nat Methods*, *14*(7), 743-751. https://doi.org/10.1038/nmeth.4304
6. Bagri, A., Marin, O., Plump, A. S., Mak, J., Pleasure, S. J., Rubenstein, J. L., & Tessier-Lavigne, M. (2002). Slit proteins prevent midline crossing and determine the dorsoventral position of major axonal pathways in the mammalian forebrain. *Neuron*, *33*(2), 233-248. https://doi.org/10.1016/s0896-6273(02)00561-5
7. Bajaj, S., Bagley, J. A., Sommer, C., Vertesy, A., Nagumo Wong, S., Krenn, V., Levi-Strauss, J., & Knoblich, J. A. (2021). Neurotransmitter signaling regulates distinct phases of multimodal human interneuron migration. *EMBO J*, *40*(23), e108714. https://doi.org/10.15252/embj.2021108714
8. Bakhru, S., Nain, A. S., Highley, C., Wang, J., Campbell, P., Amon, C., & Zappe, S. (2011). Direct and cell signaling-based, geometry-induced neuronal differentiation of neural stem cells. *Integr Biol (Camb)*, *3*(12), 1207-1214. https://doi.org/10.1039/c1ib00098e
9. Barros, C. S., Calabrese, B., Chamero, P., Roberts, A. J., Korzus, E., Lloyd, K., Stowers, L., Mayford, M., Halpain, S., & Muller, U. (2009). Impaired maturation of dendritic spines without disorganization of cortical cell layers in mice lacking NRG1/ErbB signaling in the central nervous system. *Proc Natl Acad Sci U S A*, *106*(11), 4507-4512. https://doi.org/10.1073/pnas.0900355106
10. Bartolini, G., Ciceri, G., & Marin, O. (2013). Integration of GABAergic interneurons into cortical cell assemblies: lessons from embryos and adults. *Neuron*, *79*(5), 849-864. https://doi.org/10.1016/j.neuron.2013.08.014

11. Batista-Brito, R., Majumdar, A., Nuno, A., Ward, C., Barnes, C., Nikouei, K., Vinck, M., & Cardin, J. A. (2023). Developmental loss of ErbB4 in PV interneurons disrupts state-dependent cortical circuit dynamics. *Mol Psychiatry*. https://doi.org/10.1038/s41380-023-02066-3
12. Bellion, A., Baudoin, J. P., Alvarez, C., Bornens, M., & Metin, C. (2005). Nucleokinesis in tangentially migrating neurons comprises two alternating phases: forward migration of the Golgi/centrosome associated with centrosome splitting and myosin contraction at the rear. *J Neurosci*, *25*(24), 5691-5699. https://doi.org/10.1523/JNEUROSCI.1030-05.2005
13. Bernard, C., Exposito-Alonso, D., Selten, M., Sanalidou, S., Hanusz-Godoy, A., Aguilera, A., Hamid, F., Oozeer, F., Maeso, P., Allison, L., Russell, M., Fleck, R. A., Rico, B., & Marin, O. (2022). Cortical wiring by synapse type-specific control of local protein synthesis. *Science*, *378*(6622), eabm7466. https://doi.org/10.1126/science.abm7466
14. Birey, F., Andersen, J., Makinson, C. D., Islam, S., Wei, W., Huber, N., Fan, H. C., Metzler, K. R. C., Panagiotakos, G., Thom, N., O'Rourke, N. A., Steinmetz, L. M., Bernstein, J. A., Hallmayer, J., Huguenard, J. R., & Pasca, S. P. (2017). Assembly of functionally integrated human forebrain spheroids. *Nature*, *545*(7652), 54-59. https://doi.org/10.1038/nature22330
15. Birey, F., Li, M. Y., Gordon, A., Thete, M. V., Valencia, A. M., Revah, O., Pasca, A. M., Geschwind, D. H., & Pasca, S. P. (2022). Dissecting the molecular basis of human interneuron migration in forebrain assembloids from Timothy syndrome. *Cell Stem Cell*, *29*(2), 248-264 e247. https://doi.org/10.1016/j.stem.2021.11.011
16. Boothe, T., Hilbert, L., Heide, M., Berninger, L., Huttner, W. B., Zaburdaev, V., Vastenhouw, N. L., Myers, E. W., Drechsel, D. N., & Rink, J. C. (2017). A tunable refractive index matching medium for live imaging cells, tissues and model organisms. *Elife*, *6*. https://doi.org/10.7554/eLife.27240
17. Boutin, M. E., Voss, T. C., Titus, S. A., Cruz-Gutierrez, K., Michael, S., & Ferrer, M. (2018). A high-throughput imaging and nuclear segmentation analysis protocol for cleared 3D culture models. *Sci Rep*, *8*(1), 11135. https://doi.org/10.1038/s41598-018-29169-0
18. Castano, J., Bueno, C., Jimenez-Delgado, S., Roca-Ho, H., Fraga, M. F., Fernandez, A. F., Nakanishi, M., Torres-Ruiz, R., Rodriguez-Perales, S., & Menendez, P. (2017). Generation and characterization of a human iPSC cell line expressing inducible Cas9 in the "safe harbor" AAVS1 locus. *Stem Cell Res*, *21*, 137-140. https://doi.org/10.1016/j.scr.2017.04.011
19. Chambers, S. M., Fasano, C. A., Papapetrou, E. P., Tomishima, M., Sadelain, M., & Studer, L. (2009). Highly efficient neural conversion of human ES and iPS cells by dual inhibition of SMAD signaling. *Nat Biotechnol*, *27*(3), 275-280. https://doi.org/10.1038/nbt.1529
20. Chen, Y. J., Zhang, M., Yin, D. M., Wen, L., Ting, A., Wang, P., Lu, Y. S., Zhu, X. H., Li, S. J., Wu, C. Y., Wang, X. M., Lai, C., Xiong, W. C., Mei, L., & Gao, T. M. (2010). ErbB4 in parvalbumin-positive interneurons is critical for neuregulin 1 regulation of long-term potentiation. *Proc Natl Acad Sci U S A*, *107*(50), 21818-21823. https://doi.org/10.1073/pnas.1010669107
21. Cueni, L., Canepari, M., Lujan, R., Emmenegger, Y., Watanabe, M., Bond, C. T., Franken, P., Adelman, J. P., & Luthi, A. (2008). T-type Ca2+ channels, SK2 channels and SERCAs gate sleep-related oscillations

in thalamic dendrites. *Nat Neurosci*, *11*(6), 683-692. https://doi.org/10.1038/nn.2124

22. Del Pino, I., Garcia-Frigola, C., Dehorter, N., Brotons-Mas, J. R., Alvarez-Salvado, E., Martinez de Lagran, M., Ciceri, G., Gabaldon, M. V., Moratal, D., Dierssen, M., Canals, S., Marin, O., & Rico, B. (2013). Erbb4 deletion from fast-spiking interneurons causes schizophrenia-like phenotypes. *Neuron*, *79*(6), 1152-1168. https://doi.org/10.1016/j.neuron.2013.07.010
23. Esumi, S., Nasu, M., Kawauchi, T., Miike, K., Morooka, K., Yanagawa, Y., Seki, T., Sakimura, K., Fukuda, T., & Tamamaki, N. (2021). Characterization and Stage-Dependent Lineage Analysis of Intermediate Progenitors of Cortical GABAergic Interneurons. *Front Neurosci*, *15*, 607908. https://doi.org/10.3389/fnins.2021.607908
24. Fazzari, P., Paternain, A. V., Valiente, M., Pla, R., Lujan, R., Lloyd, K., Lerma, J., Marin, O., & Rico, B. (2010). Control of cortical GABA circuitry development by Nrg1 and ErbB4 signalling. *Nature*, *464*(7293), 1376-1380. https://doi.org/10.1038/nature08928
25. Flames, N., Long, J. E., Garratt, A. N., Fischer, T. M., Gassmann, M., Birchmeier, C., Lai, C., Rubenstein, J. L., & Marin, O. (2004). Short- and long-range attraction of cortical GABAergic interneurons by neuregulin-1. *Neuron*, *44*(2), 251-261. https://doi.org/10.1016/j.neuron.2004.09.028
26. Gambarotta, G., Garzotto, D., Destro, E., Mautino, B., Giampietro, C., Cutrupi, S., Dati, C., Cattaneo, E., Fasolo, A., & Perroteau, I. (2004). ErbB4 expression in neural progenitor cells (ST14A) is necessary to mediate neuregulin-1beta1-induced migration. *J Biol Chem*, *279*(47), 48808-48816. https://doi.org/10.1074/jbc.M408374200
27. Gassmann, M., Casagranda, F., Orioli, D., Simon, H., Lai, C., Klein, R., & Lemke, G. (1995). Aberrant neural and cardiac development in mice lacking the ErbB4 neuregulin receptor. *Nature*, *378*(6555), 390-394. https://doi.org/10.1038/378390a0
28. Gillespie, M., Jassal, B., Stephan, R., Milacic, M., Rothfels, K., Senff-Ribeiro, A., Griss, J., Sevilla, C., Matthews, L., Gong, C., Deng, C., Varusai, T., Ragueneau, E., Haider, Y., May, B., Shamovsky, V., Weiser, J., Brunson, T., Sanati, N., . . . D'Eustachio, P. (2022). The reactome pathway knowledgebase 2022. *Nucleic Acids Res*, *50*(D1), D687-D692. https://doi.org/10.1093/nar/gkab1028
29. He, Z., Maynard, A., Jain, A., Gerber, T., Petri, R., Lin, H. C., Santel, M., Ly, K., Dupre, J. S., Sidow, L., Sanchis Calleja, F., Jansen, S. M. J., Riesenberg, S., Camp, J. G., & Treutlein, B. (2022). Lineage recording in human cerebral organoids. *Nat Methods*, *19*(1), 90-99. https://doi.org/10.1038/s41592-021-01344-8
30. Hodge, R. D., Bakken, T. E., Miller, J. A., Smith, K. A., Barkan, E. R., Graybuck, L. T., Close, J. L., Long, B., Johansen, N., Penn, O., Yao, Z., Eggermont, J., Hollt, T., Levi, B. P., Shehata, S. I., Aevermann, B., Beller, A., Bertagnolli, D., Brouner, K., . . . Lein, E. S. (2019). Conserved cell types with divergent features in human versus mouse cortex. *Nature*, *573*(7772), 61-68. https://doi.org/10.1038/s41586-019-1506-7
31. Hyder, Z., Van Paesschen, W., Sabir, A., Sansbury, F. H., Burke, K. B., Khan, N., Chandler, K. E., Cooper, N. S., Wright, R., McHale, E., Van Esch, H., & Banka, S. (2021). ERBB4 exonic deletions on chromosome 2q34 in patients with intellectual disability or epilepsy. *Eur J Hum Genet*, *29*(9), 1377-1383. https://doi.org/10.1038/s41431-021-00815-y

32. Inada, H., Watanabe, M., Uchida, T., Ishibashi, H., Wake, H., Nemoto, T., Yanagawa, Y., Fukuda, A., & Nabekura, J. (2011). GABA regulates the multidirectional tangential migration of GABAergic interneurons in living neonatal mice. *PLoS One*, *6*(12), e27048. https://doi.org/10.1371/journal.pone.0027048
33. Jana, A., Nookaew, I., Singh, J., Behkam, B., Franco, A. T., & Nain, A. S. (2019). Crosshatch nanofiber networks of tunable interfiber spacing induce plasticity in cell migration and cytoskeletal response. *FASEB J*, *33*(10), 10618-10632. https://doi.org/10.1096/fj.201900131R
34. Jana, A., Sarkar, A., Zhang, H., Agashe, A., Wang, J., Paul, R., Gov, N. S., DeLuca, J. G., & Nain, A. S. (2023). Mitotic outcomes and errors in fibrous environments. *Proc Natl Acad Sci U S A*, *120*(10), e2120536120. https://doi.org/10.1073/pnas.2120536120
35. Jovanov Milosevic, N., Judas, M., Aronica, E., & Kostovic, I. (2014). Neural ECM in laminar organization and connectivity development in healthy and diseased human brain. *Prog Brain Res*, *214*, 159-178. https://doi.org/10.1016/B978-0-444-63486-3.00007-4
36. Kainulainen, V., Sundvall, M., Maatta, J. A., Santiestevan, E., Klagsbrun, M., & Elenius, K. (2000). A natural ErbB4 isoform that does not activate phosphoinositide 3-kinase mediates proliferation but not survival or chemotaxis. *J Biol Chem*, *275*(12), 8641-8649. https://doi.org/10.1074/jbc.275.12.8641
37. Kasnauskiene, J., Ciuladaite, Z., Preiksaitiene, E., Utkus, A., Peciulyte, A., & Kucinskas, V. (2013). A new single gene deletion on 2q34: ERBB4 is associated with intellectual disability. *Am J Med Genet A*, *161A*(6), 1487-1490. https://doi.org/10.1002/ajmg.a.35911
38. Kiral, F. R., Cakir, B., Tanaka, Y., Kim, J., Yang, W. S., Wehbe, F., Kang, Y. J., Zhong, M., Sancer, G., Lee, S. H., Xiang, Y., & Park, I. H. (2023). Generation of ventralized human thalamic organoids with thalamic reticular nucleus. *Cell Stem Cell*, *30*(5), 677-688 e675. https://doi.org/10.1016/j.stem.2023.03.007
39. Lancaster, M. A., & Knoblich, J. A. (2014). Generation of cerebral organoids from human pluripotent stem cells. *Nat Protoc*, *9*(10), 2329-2340. https://doi.org/10.1038/nprot.2014.158
40. Lancaster, M. A., Renner, M., Martin, C. A., Wenzel, D., Bicknell, L. S., Hurles, M. E., Homfray, T., Penninger, J. M., Jackson, A. P., & Knoblich, J. A. (2013). Cerebral organoids model human brain development and microcephaly. *Nature*, *501*(7467), 373-379. https://doi.org/10.1038/nature12517
41. Lepiemme, F., Stoufflet, J., Javier-Torrent, M., Mazzucchelli, G., Silva, C. G., & Nguyen, L. (2022). Oligodendrocyte precursors guide interneuron migration by unidirectional contact repulsion. *Science*, *376*(6595), eabn6204. https://doi.org/10.1126/science.abn6204
42. Liang, X., Draghi, N. A., & Resh, M. D. (2004). Signaling from integrins to Fyn to Rho family GTPases regulates morphologic differentiation of oligodendrocytes. *J Neurosci*, *24*(32), 7140-7149. https://doi.org/10.1523/JNEUROSCI.5319-03.2004
43. Liu, X., Lu, Y., Zhang, Y., Li, Y., Zhou, J., Yuan, Y., Gao, X., Su, Z., & He, C. (2012). Slit2 regulates the dispersal of oligodendrocyte precursor cells via Fyn/RhoA signaling. *J Biol Chem*, *287*(21), 17503-17516. https://doi.org/10.1074/jbc.M111.317610

44. Luo, B., Liu, Z., Lin, D., Chen, W., Ren, D., Yu, Z., Xiong, M., Zhao, C., Fei, E., & Li, B. (2021). ErbB4 promotes inhibitory synapse formation by cell adhesion, independent of its kinase activity. *Transl Psychiatry*, *11*(1), 361. https://doi.org/10.1038/s41398-021-01485-6
45. Ma, T., Wang, C., Wang, L., Zhou, X., Tian, M., Zhang, Q., Zhang, Y., Li, J., Liu, Z., Cai, Y., Liu, F., You, Y., Chen, C., Campbell, K., Song, H., Ma, L., Rubenstein, J. L., & Yang, Z. (2013). Subcortical origins of human and monkey neocortical interneurons. *Nat Neurosci*, *16*(11), 1588-1597. https://doi.org/10.1038/nn.3536
46. Mali, P., Yang, L., Esvelt, K. M., Aach, J., Guell, M., DiCarlo, J. E., Norville, J. E., & Church, G. M. (2013). RNA-guided human genome engineering via Cas9. *Science*, *339*(6121), 823-826. https://doi.org/10.1126/science.1232033
47. Marin, O. (2012). Interneuron dysfunction in psychiatric disorders. *Nat Rev Neurosci*, *13*(2), 107-120. https://doi.org/10.1038/nrn3155
48. Marin, O., Plump, A. S., Flames, N., Sanchez-Camacho, C., Tessier-Lavigne, M., & Rubenstein, J. L. (2003). Directional guidance of interneuron migration to the cerebral cortex relies on subcortical Slit1/2-independent repulsion and cortical attraction. *Development*, *130*(9), 1889-1901. https://doi.org/10.1242/dev.00417
49. Martinez-Martinez, M. A., Ciceri, G., Espinos, A., Fernandez, V., Marin, O., & Borrell, V. (2019). Extensive branching of radially-migrating neurons in the mammalian cerebral cortex. *J Comp Neurol*, *527*(10), 1558-1576. https://doi.org/10.1002/cne.24597
50. Mayer, C., Hafemeister, C., Bandler, R. C., Machold, R., Batista Brito, R., Jaglin, X., Allaway, K., Butler, A., Fishell, G., & Satija, R. (2018). Developmental diversification of cortical inhibitory interneurons. *Nature*, *555*(7697), 457-462. https://doi.org/10.1038/nature25999
51. Mei, L., & Xiong, W. C. (2008). Neuregulin 1 in neural development, synaptic plasticity and schizophrenia. *Nat Rev Neurosci*, *9*(6), 437-452. https://doi.org/10.1038/nrn2392
52. Meng, X., Yao, D., Imaizumi, K., Chen, X., Kelley, K. W., Reis, N., Thete, M. V., Arjun McKinney, A., Kulkarni, S., Panagiotakos, G., Bassik, M. C., & Pasca, S. P. (2023). Assembloid CRISPR screens reveal impact of disease genes in human neurodevelopment. *Nature*, *622*(7982), 359-366. https://doi.org/10.1038/s41586-023-06564-w
53. Mukherjee, A., Ron, J. E., Hu, H. T., Nishimura, T., Hanawa-Suetsugu, K., Behkam, B., Mimori-Kiyosue, Y., Gov, N. S., Suetsugu, S., & Nain, A. S. (2023). Actin Filaments Couple the Protrusive Tips to the Nucleus through the I-BAR Domain Protein IRSp53 during the Migration of Cells on 1D Fibers. *Adv Sci (Weinh)*, *10*(7), e2207368. https://doi.org/10.1002/advs.202207368
54. Neddens, J., & Buonanno, A. (2010). Selective populations of hippocampal interneurons express ErbB4 and their number and distribution is altered in ErbB4 knockout mice. *Hippocampus*, *20*(6), 724-744. https://doi.org/10.1002/hipo.20675
55. Nichols, A. J., Carney, L. H., & Olson, E. C. (2008). Comparison of slow and fast neocortical neuron migration using a new in vitro model. *BMC Neurosci*, *9*, 50. https://doi.org/10.1186/1471-2202-9-50

56. Pasca, A. M., Sloan, S. A., Clarke, L. E., Tian, Y., Makinson, C. D., Huber, N., Kim, C. H., Park, J. Y., O'Rourke, N. A., Nguyen, K. D., Smith, S. J., Huguenard, J. R., Geschwind, D. H., Barres, B. A., & Pasca, S. P. (2015). Functional cortical neurons and astrocytes from human pluripotent stem cells in 3D culture. *Nat Methods*, *12*(7), 671-678. https://doi.org/10.1038/nmeth.3415
57. Peyre, E., Silva, C. G., & Nguyen, L. (2015). Crosstalk between intracellular and extracellular signals regulating interneuron production, migration and integration into the cortex. *Front Cell Neurosci*, *9*, 129. https://doi.org/10.3389/fncel.2015.00129
58. Pinal, C. S., & Tobin, A. J. (1998). Uniqueness and redundancy in GABA production. *Perspect Dev Neurobiol*, *5*(2-3), 109-118. https://www.ncbi.nlm.nih.gov/pubmed/9777629
59. Quadrato, G., Nguyen, T., Macosko, E. Z., Sherwood, J. L., Min Yang, S., Berger, D. R., Maria, N., Scholvin, J., Goldman, M., Kinney, J. P., Boyden, E. S., Lichtman, J. W., Williams, Z. M., McCarroll, S. A., & Arlotta, P. (2017). Cell diversity and network dynamics in photosensitive human brain organoids. *Nature*, *545*(7652), 48-53. https://doi.org/10.1038/nature22047
60. Rakic, S., Kanatani, S., Hunt, D., Faux, C., Cariboni, A., Chiara, F., Khan, S., Wansbury, O., Howard, B., Nakajima, K., Nikolic, M., & Parnavelas, J. G. (2015). Cdk5 phosphorylation of ErbB4 is required for tangential migration of cortical interneurons. *Cereb Cortex*, *25*(4), 991-1003. https://doi.org/10.1093/cercor/bht290
61. Revell, C. K., Jensen, O. E., Shearer, T., Lu, Y., Holmes, D. F., & Kadler, K. E. (2021). Collagen fibril assembly: New approaches to unanswered questions. *Matrix Biol Plus*, *12*, 100079. https://doi.org/10.1016/j.mbplus.2021.100079
62. Shamir, A., Kwon, O. B., Karavanova, I., Vullhorst, D., Leiva-Salcedo, E., Janssen, M. J., & Buonanno, A. (2012). The importance of the NRG-1/ErbB4 pathway for synaptic plasticity and behaviors associated with psychiatric disorders. *J Neurosci*, *32*(9), 2988-2997. https://doi.org/10.1523/JNEUROSCI.1899-11.2012
63. Siadat, S. M., Silverman, A. A., DiMarzio, C. A., & Ruberti, J. W. (2021). Measuring collagen fibril diameter with differential interference contrast microscopy. *J Struct Biol*, *213*(1), 107697. https://doi.org/10.1016/j.jsb.2021.107697
64. Silbereis, J. C., Pochareddy, S., Zhu, Y., Li, M., & Sestan, N. (2016). The Cellular and Molecular Landscapes of the Developing Human Central Nervous System. *Neuron*, *89*(2), 248-268. https://doi.org/10.1016/j.neuron.2015.12.008
65. Sloan, S. A., Andersen, J., Pasca, A. M., Birey, F., & Pasca, S. P. (2018). Generation and assembly of human brain region-specific three-dimensional cultures. *Nat Protoc*, *13*(9), 2062-2085. https://doi.org/10.1038/s41596-018-0032-7
66. Sundvall, M., Korhonen, A., Paatero, I., Gaudio, E., Melino, G., Croce, C. M., Aqeilan, R. I., & Elenius, K. (2008). Isoform-specific monoubiquitination, endocytosis, and degradation of alternatively spliced ErbB4 isoforms. *Proc Natl Acad Sci U S A*, *105*(11), 4162-4167. https://doi.org/10.1073/pnas.0708333105

67. Sykova, E., & Nicholson, C. (2008). Diffusion in brain extracellular space. *Physiol Rev*, *88*(4), 1277-1340. https://doi.org/10.1152/physrev.00027.2007

68. Tamamaki, N., Yanagawa, Y., Tomioka, R., Miyazaki, J., Obata, K., & Kaneko, T. (2003). Green fluorescent protein expression and colocalization with calretinin, parvalbumin, and somatostatin in the GAD67-GFP knock-in mouse. *J Comp Neurol*, *467*(1), 60-79. https://doi.org/10.1002/cne.10905

69. Tanaka, D. H., Yanagida, M., Zhu, Y., Mikami, S., Nagasawa, T., Miyazaki, J., Yanagawa, Y., Obata, K., & Murakami, F. (2009). Random walk behavior of migrating cortical interneurons in the marginal zone: time-lapse analysis in flat-mount cortex. *J Neurosci*, *29*(5), 1300-1311. https://doi.org/10.1523/JNEUROSCI.5446-08.2009

70. Tatti, R., Haley, M. S., Swanson, O. K., Tselha, T., & Maffei, A. (2017). Neurophysiology and Regulation of the Balance Between Excitation and Inhibition in Neocortical Circuits. *Biol Psychiatry*, *81*(10), 821-831. https://doi.org/10.1016/j.biopsych.2016.09.017

71. Tsai, J. W., Bremner, K. H., & Vallee, R. B. (2007). Dual subcellular roles for LIS1 and dynein in radial neuronal migration in live brain tissue. *Nat Neurosci*, *10*(8), 970-979. https://doi.org/10.1038/nn1934

72. van Helvert, S., & Friedl, P. (2016). Strain Stiffening of Fibrillar Collagen during Individual and Collective Cell Migration Identified by AFM Nanoindentation. *ACS Appl Mater Interfaces*, *8*(34), 21946-21955. https://doi.org/10.1021/acsami.6b01755

73. Vullhorst, D., Neddens, J., Karavanova, I., Tricoire, L., Petralia, R. S., McBain, C. J., & Buonanno, A. (2009). Selective expression of ErbB4 in interneurons, but not pyramidal cells, of the rodent hippocampus. *J Neurosci*, *29*(39), 12255-12264. https://doi.org/10.1523/JNEUROSCI.2454-09.2009

74. Wen, L., Lu, Y. S., Zhu, X. H., Li, X. M., Woo, R. S., Chen, Y. J., Yin, D. M., Lai, C., Terry, A. V., Jr., Vazdarjanova, A., Xiong, W. C., & Mei, L. (2010). Neuregulin 1 regulates pyramidal neuron activity via ErbB4 in parvalbumin-positive interneurons. *Proc Natl Acad Sci U S A*, *107*(3), 1211-1216. https://doi.org/10.1073/pnas.0910302107

75. Won, C., Lin, Z., Kumar, T. P., Li, S., Ding, L., Elkhal, A., Szabo, G., & Vasudevan, A. (2013). Autonomous vascular networks synchronize GABA neuron migration in the embryonic forebrain. *Nat Commun*, *4*, 2149. https://doi.org/10.1038/ncomms3149

76. Wong, K., Ren, X. R., Huang, Y. Z., Xie, Y., Liu, G., Saito, H., Tang, H., Wen, L., Brady-Kalnay, S. M., Mei, L., Wu, J. Y., Xiong, W. C., & Rao, Y. (2001). Signal transduction in neuronal migration: roles of GTPase activating proteins and the small GTPase Cdc42 in the Slit-Robo pathway. *Cell*, *107*(2), 209-221. https://doi.org/10.1016/s0092-8674(01)00530-x

77. Yanagida, M., Miyoshi, R., Toyokuni, R., Zhu, Y., & Murakami, F. (2012). Dynamics of the leading process, nucleus, and Golgi apparatus of migrating cortical interneurons in living mouse embryos. *Proc Natl Acad Sci U S A*, *109*(41), 16737-16742. https://doi.org/10.1073/pnas.1209166109

78. Yeo, M. G., Oh, H. J., Cho, H. S., Chun, J. S., Marcantonio, E. E., & Song, W. K. (2011). Phosphorylation of Ser 21 in Fyn regulates its kinase activity, focal adhesion targeting, and is required for cell migration. *J Cell Physiol*, *226*(1), 236-247. https://doi.org/10.1002/jcp.22335

79. Yokota, Y., Gashghaei, H. T., Han, C., Watson, H., Campbell, K. J., & Anton, E. S. (2007). Radial glial dependent and independent dynamics of interneuronal migration in the developing cerebral cortex. *PLoS One*, *2*(8), e794. https://doi.org/10.1371/journal.pone.0000794
80. Yoon, S. J., Elahi, L. S., Pasca, A. M., Marton, R. M., Gordon, A., Revah, O., Miura, Y., Walczak, E. M., Holdgate, G. M., Fan, H. C., Huguenard, J. R., Geschwind, D. H., & Pasca, S. P. (2019). Reliability of human cortical organoid generation. *Nat Methods*, *16*(1), 75-78. https://doi.org/10.1038/s41592-018-0255-0
81. Yun, K., Fischman, S., Johnson, J., Hrabe de Angelis, M., Weinmaster, G., & Rubenstein, J. L. (2002). Modulation of the notch signaling by Mash1 and Dlx1/2 regulates sequential specification and differentiation of progenitor cell types in the subcortical telencephalon. *Development*, *129*(21), 5029-5040. https://doi.org/10.1242/dev.129.21.5029

Supplementary Information

Supplementary Movies 1 to 11, Supplementary Data Files 1 to 4, and Supplementary Tables 1 and 2 are not available with this version.

Figures

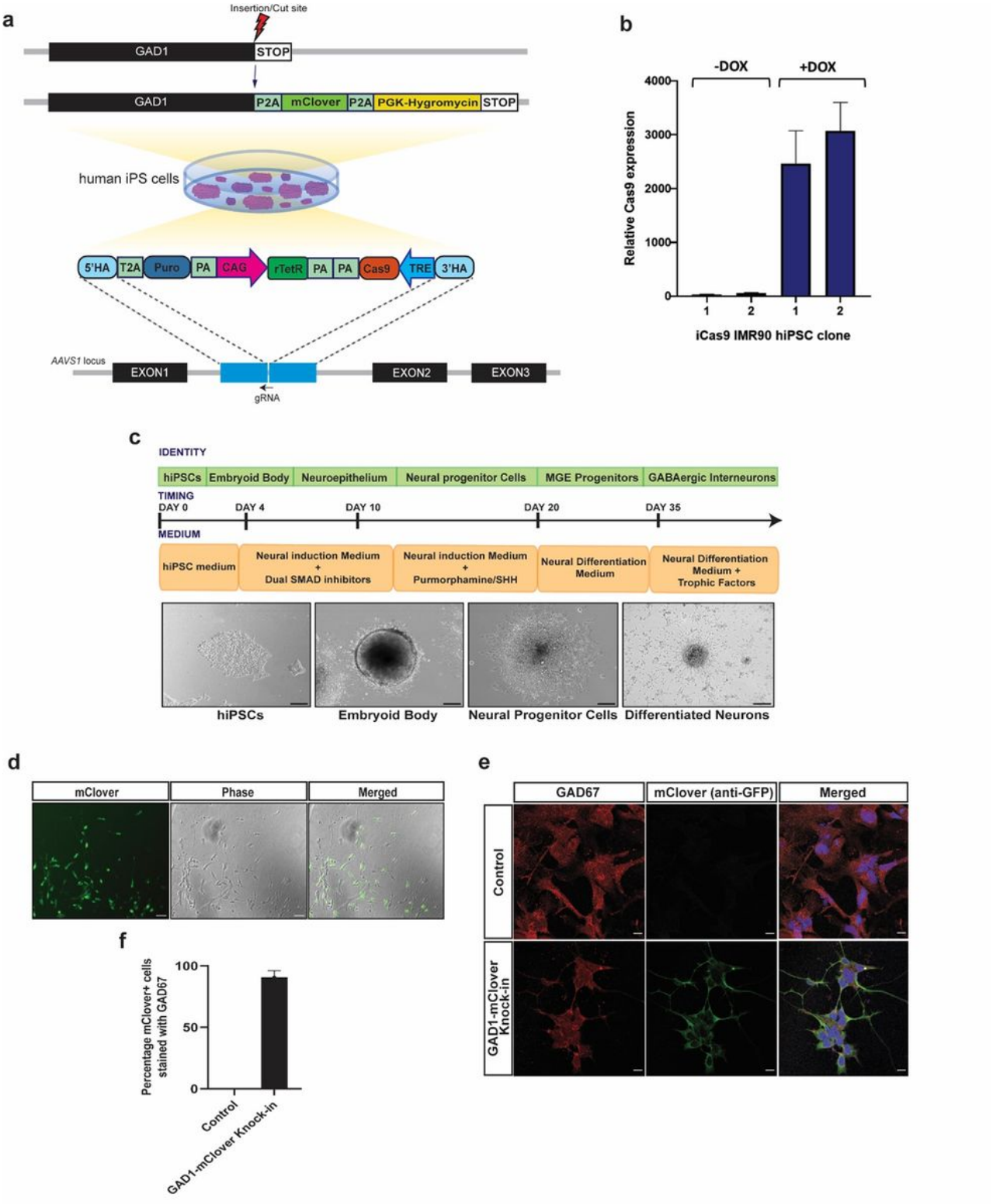

Figure 1

GAD1-mClover reporter identifies migrating human interneurons.

a) Schematic for knock-in of inducible Cas9 and Cas9 mediated HDR and knockin of mClover fluorophore into the GAD1 locus in hiPSCs. 7.7 kb donor DNA cassette was used for HDR at the AAVS1 locus and a TET-ON system employed for SpCas9 expression upon doxycycline treatment. Puro: Puromycin; T2A:

Thoseaasigna virus 2A; PA: porcine teschovirus-1 2A; CAG: CMV immediate enhancer/β-actin promoter; TRE: Tetracycline Response Element; rTetR:.reverse tetracycline repressor; HA: Homology Arm.

b) qRT-PCR for expression check of Cas9 transcript levels with and without doxycycline treatment (2ug/ml) in clone 1 and 2 of iCas9-IMR90 hiPS lines.

c) Timeline of differentiation of GABAergic interneurons from hiPSCs. The Embryoid Body (EB) derived from hiPSCs are plated on day 7. By day 10, each EB will develop into a colony that contains neuroepithelial cells. Scale:100 μm

d) Stable reporter signal in live Gad1-mClover neurons in culture. Scale, 50 μm, 20x magnification.

e) Representative immunofluorescence images of Day 50 neuronal cultures derived from control iCas9 IMR90 iPSCs and GAD1-mClover knock-in iCas9 IMR90 hiPSCs (63x mag., Scale: 10 μm)

f) Quantification of mClover positive cells stained for GAD67. Data is represented as mean ±S.D. (n=3 individual cell differentiation batches).

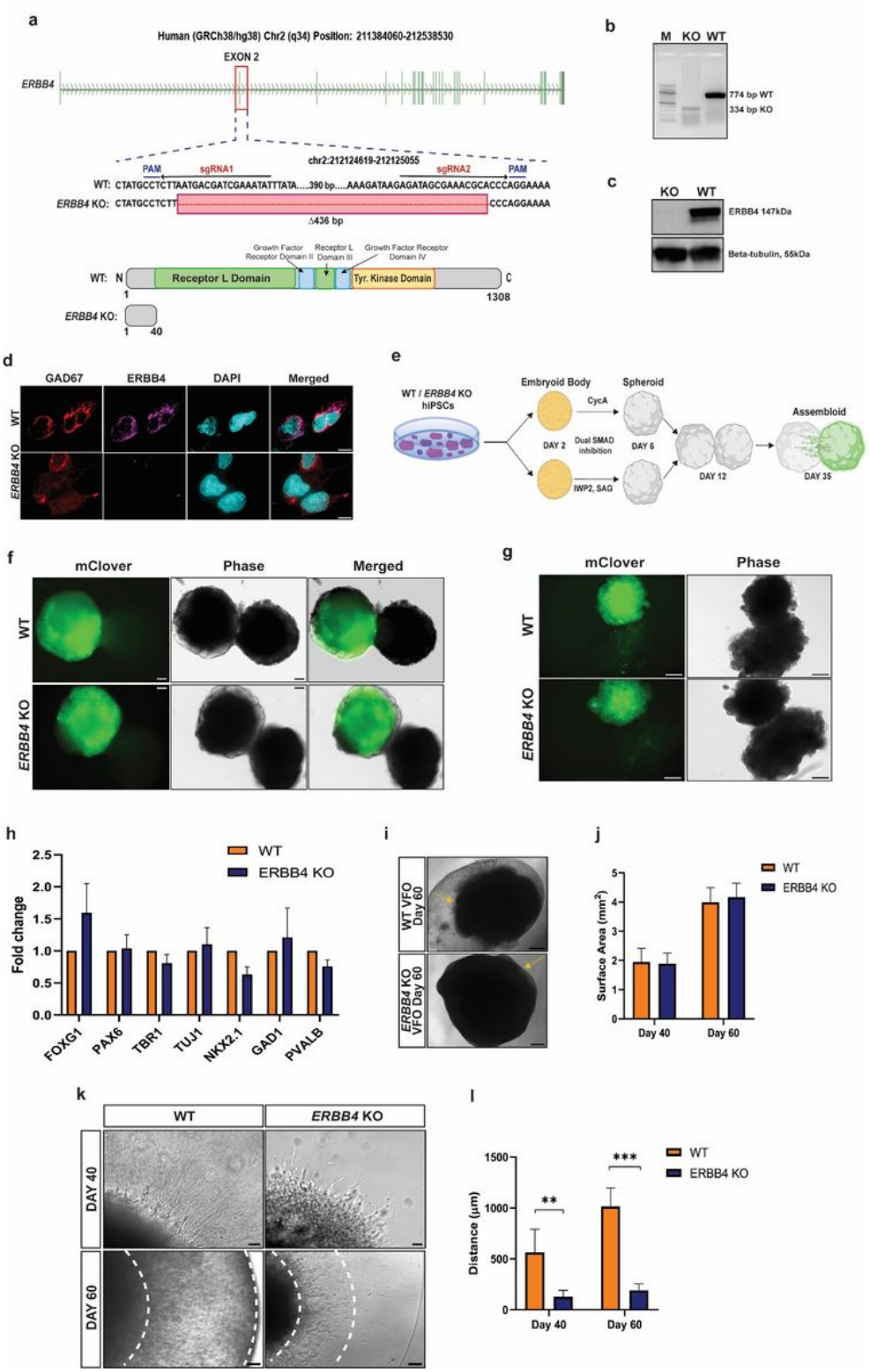

Figure 2

Generation of region-specific forebrain assembloids.

a) Schematic illustrating human ERBB4 gene structure and protein domains. Red rectangle denotes exon 2 which is missing in the deletion lines. Sequence of the representative deletion fragment of ERBB4 (436 bp). PAM in blue, sgRNA are in red, and deleted bases are replaced by red dash in Knockout (KO).

b) Genotyping PCR for exon 2 deletion in a single hiPS colony.

c) Western Blot analysis of ERBB4 protein expression in differentiated neurons. Lysates from day 35 culture neurons (ERBB4 KO and wildtype) were probed using anti-ERBB4 antibody on western blot with beta-Tubulin as loading control.

d) Immunofluorescence images of WT and ERBB4 knockout neurons stained for GAD67 (red), ERBB4 (magenta) and DAPI, 60x mag., Scale: 10 µm.

e) Schematic of the timeline and small molecule treatment before fusion of forebrain organoids.

f) Representative phase and mClover (GFP) images of WT and ERBB4 KO fused assembloids in culture at day 30 with endogenous fluorescent signal from one half only. Scale: 50 µm.

g) Representative images of fused assembloids at day 50 in culture with mClover+ cells migrated across the boundary of the ventral organoids ahead of the fusion zone towards the unlabeled region. Scale: 100 µm

h) qPCR analysis for expression of lineage markers in WT and ERBB4 KO ventral:dorsal fused assembloids (day 50). Values are plotted as fold change expression over WT and normalized to the reference gene GAPDH. Data represents mean ±S.D, n=3. Unpaired two-tailed Student's t-test was performed with non-significant (p-value>0.05) result across all individual comparisons.

i) Representative phase contrast images of VFO on day 60 in culture with WT showing extensive neuronal projections (yellow arrow) outside the perimeter of the organoid while ERBB4 KO with visibly reduced projections. Scale: 100 µm

j) Quantification of surface area (mm2) of organoids from the images at day 40 and day 60 for 15 organoids from WT and ERBB4 KO (3 independent batches), data represents mean ± S.D.

k) Representative brightfield images of a part of VFO at day 40 and day 60 in culture showing neuronal projections inside matrigel droplet. Scale: 100 µm. White dashed lines mark the area with projections used for quantification of radial migration distance in (l).

l) Quantification of migration distance from periphery of VFO. Data represents mean ± S.D with unpaired two-tailed Student's t-test, ** for p-value ≤ 0.01 and *** for p-value ≤ 0.001.

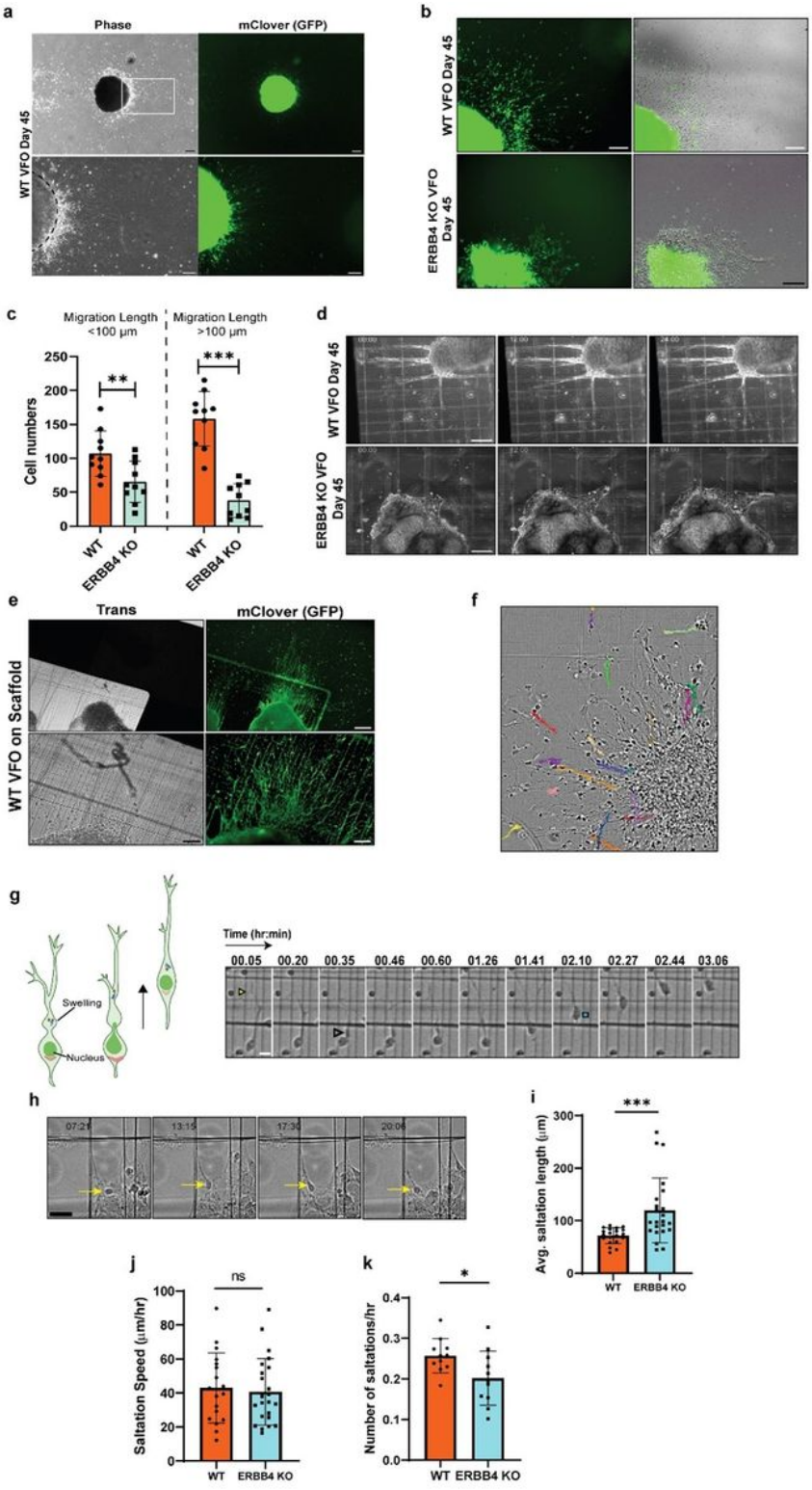

Figure 3

in vitro migration assay of CINs from ventral forebrain organoids.

a) Representative image of WT VFO, 3 days post-plating on coverslip, inset from selected region of upper panel (white rectangle) at higher magnification shows mClover+ interneurons migrating out of the organoid perimeter (black dashed lines) Scale bar: 50 µm.

b) Representative panel of WT and KO organoids displaying differences in the migration of mClover+ cells as KO interneurons show lack of individual long projections and do not escape far from periphery. Scale bar: 50 μm.

c) Quantification of number of interneurons migrating till 100 μm and more than 100 μm from WT and *ERBB4* KO VFOS. Data represents mean ± S.D. Unpaired two-tailed Student's t-test was performed for statistical significance, ** indicates p-value < 0.01 and *** indicates p-value < 0.001.

d) Representative phase images from time series (hr:min) imaging of WT VFO and ERBB4 KO VFO sample on force scaffold with 500nm thick fibers having 180 μm fiber spacing, imaged using 10x objective with digital zoom (3x), Scale: 100 μm. WT sample shows extended neurites while collective migration and reduced projections visible in ERBB4 KO.

e) Micrographs of a WT VFO fixed and stained for GFP (mClover) on migration scaffold showing extensive interneuron migration and spread (yellow arrow in upper panel) post 3 days of attachment on fibers. Upper panel: 4x magnification, Scale: 100 μm, lower panel: 10x magnification, Scale: 50 μm.

f) Migration tracks of individual interneurons traced through time-lapse sequence of imaging till 9 hrs. Individual tracks are highlighted by different colors.

g) CINs display saltatory mode of movement on scaffolds. (i) Schematic showing nucleokinesis (jumping of nucleus) event during interneuron migration which is preceded by the formation of a swelling in soma region behind leading branches. (ii) Representative images of one complete nuclear translocation displayed by a WT interneuron on scaffold at different time points showing a branched leading process with extending growth cone (yellow closed arrowhead) and swelling ahead of the nucleus is denoted by open arrowhead (black). Nuclear translocation (blue square) is saltatory. Scale bar: 10 μm.

h) Representative phase images from the time series highlighting the inability of ERBB4 KO interneuron (yellow arrow on all frames) in migrating forward, Scale: 50 μm.

i) Quantification of length of a single saltation (μm) by WT and *ERBB4* KO CINs. Mann Whitney non-parametric test was performed for statistical significance, *** indicates p-value: 0.0001.

j) Quantification of saltation speed (speed when mobile) of interneurons in μm/hr. Unpaired two-tailed Student's t-test was performed for statistical significance, ns: not significant.

k) Quantification of frequency of saltations by WT and *ERBB4* KO CINs. Unpaired two-tailed Student's t-test was performed for statistical significance, *p-value: 0.0316

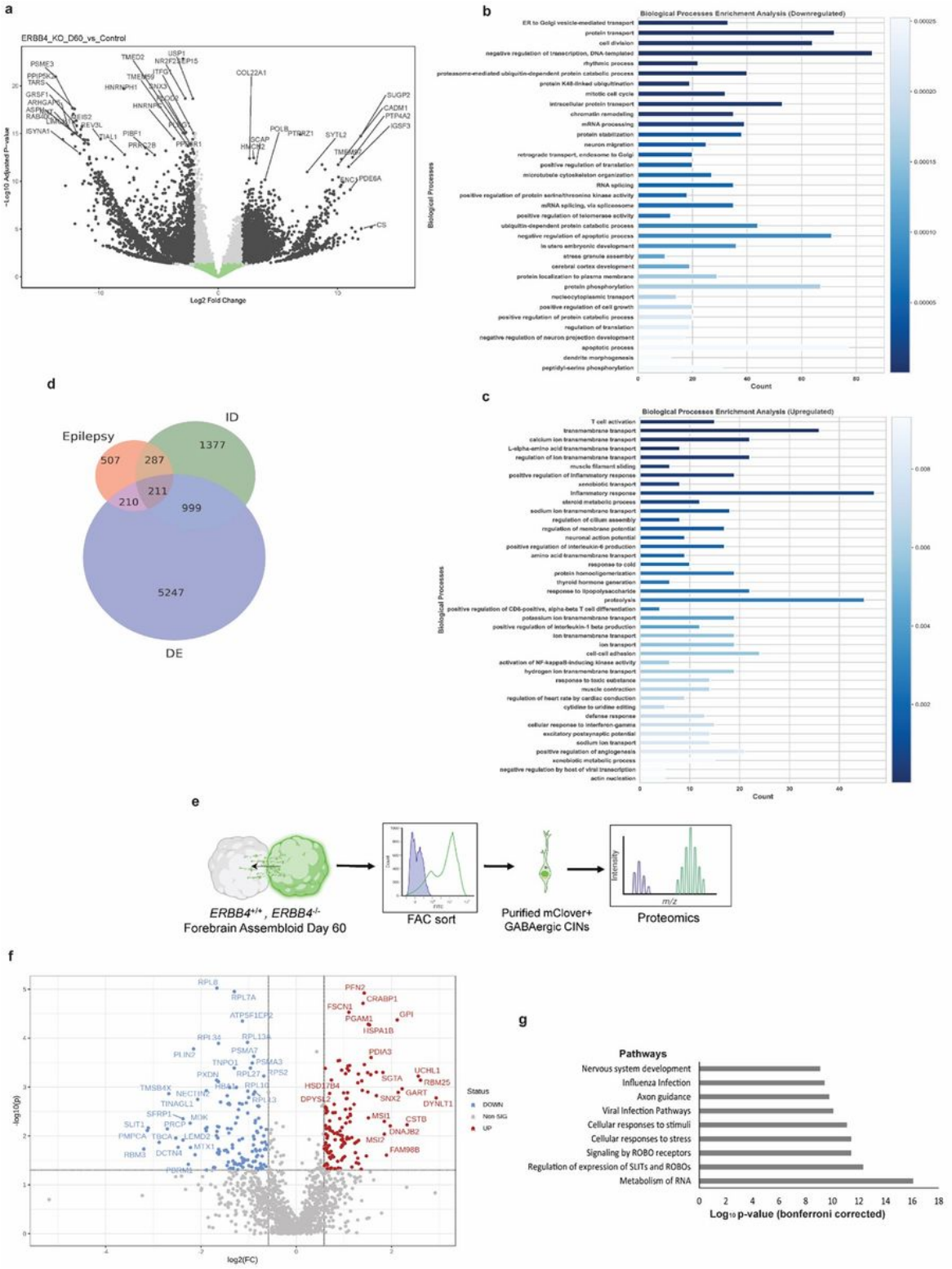

Figure 4

RHOA/RAC signaling pathway is dysregulated in *ERBB4* KO assembloids.

a) Volcano plot showing genes downregulated and upregulated in the *ERBB4*$^{-/-}$ assembloids, day 60 (log2 fold change>2 and false discovery rate (FDR) <0.05; p-value<0.001). Top altered gene symbols are marked and non-significant genes are colored in grey.

b-c) Gene ontology (GO) enrichment analysis. Graphs showing Biological Processes terms enriched in genes downregulated (i) or upregulated (ii) in the *ERBB4*$^{-/-}$ assembloids according to significance (p-value) depicted in the bar color and bar length corresponds to identified gene counts in the pathway.

d) Enrichment of Intellectual Disability (ID) and epilepsy risk genes in differentially expressed (DE) genes (blue shading) in *ERBB4*$^{-/-}$ assembloids. Overlaps between data are displayed as Venn diagrams and Two-sided Fisher's Exact Test was used to determine if DE genes show enrichment in ID and epilepsy database lists. DE/ID: Fold Enrichment: 0.88 and p-value: 7.92x10-10; DE/Epilepsy Fold Enrichment: 0.82 and p-value: 2.36x 10-8.

e) Schematic for proteomic profiling from WT (*ERBB4*$^{+/+}$) and *ERBB4* KO (*ERBB4*$^{-/-}$) CINs after dissociation of assembloids and FACs sorting.

f) Volcano plot showing proteins downregulated (blue) and upregulated (red) in the *ERBB4*$^{-/-}$ CINs, day 60 (Fold change cut off = ±1.5; p-value < 0.05). Top altered gene symbols are marked and non-significant proteins are colored in grey.

g) Gene ontology (GO) enrichment analysis showing pathway terms enriched in the *ERBB4*$^{-/-}$ CINs according to significance (p-value) depicted on the x-axis.

Supplementary Files

This is a list of supplementary files associated with this preprint. Click to download.

- SupplementaryFigures.docx